Chair of Electrical Engineering

Master's Thesis

Measurement and Hardware Simulation on Torque, Speed & Load of a Prime Mover for optimization of a Sucker Rod Pumping System

Christopher Bode, BSc

September 2019

B.Sc. Christopher Bode

Master Thesis 2018/19 supervised by
Univ. Prof. Dipl.-Ing. Dr. techn. Weiß Helmut

Measurement and Hardware Simulation on Torque, Speed & Load of a Prime Mover for Optimization of a Sucker Rod Pumping System

OMV
dpe DEPARTMENT PETROLEUM ENGINEERING
iET Institute für Elektrotechnik
MONTAN UNIVERSITÄT

This Thesis is dedicated to Erika Ingami who always believed in me and pushed me to be better and to my parents for their continued support.

Eidesstattliche Erklärung

Ich erkläre an Eides statt, dass ich diese Arbeit selbständig verfasst, andere als die angegebenen Quellen und Hilfsmittel nicht benutzt, und mich auch sonst keiner unerlaubten Hilfsmittel bedient habe.

Ich erkläre, dass ich die Richtlinien des Senats der Montanuniversität Leoben zu "Gute wissenschaftliche Praxis" gelesen, verstanden und befolgt habe.

Weiters erkläre ich, dass die elektronische und gedruckte Version der eingereichten wissenschaftlichen Abschlussarbeit formal und inhaltlich identisch sind.

_____

Christopher Bode, 26 September 2019

00835345

Abstract

In the Oil and Gas industry 3 phase squirrel cage induction motors are commonly used for powering sucker rod pumps. In order to identify potential optimization of the pumping jack prime mover for field operations, a testing facility is required for analysing the performance of the engine in a controlled and safe environment.

The thesis focuses on the steps that have been taken to build up a test stand to simulate the operational strain that the induction motor is subjected to during production operation.

The testing is performed by connecting a prime mover to a second engine that simulates the torque that is applied to the engine while pumping oil to the surface. In addition to the VSD drives that each engine is equipped with, a control unit had to be introduced to the second motor to display the characteristic torque of the pumping simulator.

A major part of the thesis illustrates the installation of a measurement system, the data acquisition phase and the means necessary for accurate data processing. The testing facility measurement instruments will provide an insight into both engines performances by analysing the current, voltage, torque, speed and position of the shaft. Furthermore, the research will also provide a more detailed insight into electric losses during certain operational states.

The test stand aims to give an insight into the 3 phase squirrel cage induction motors capacity and potential by providing a specific torque scenario through the pump simulator. Consequently, the testing allows to identify the parameters to optimize an induction motor into a more energy efficient prime mover.

Zusammenfassung

In der Öl- und Gasindustrie werden üblicherweise 3-Phasen-Käfigläufermotoren zum Antrieb von Pferdekopfpumpen verwendet. Um potentielle Optimierungen des Pumpen - Antriebsaggregats für den Feldeinsatz zu identifizieren, ist eine Testanlage erforderlich, um die Leistung des Motors in einer kontrollierten und sicheren Umgebung zu analysieren und zu testen.

Die Arbeit konzentriert sich auf die Schritte, die zum Aufbau eines Prüfstandes unternommen wurden, um die Betriebsbelastung zu simulieren, der der Induktionsmotor während des Produktionsbetriebs ausgesetzt ist.

Die Prüfung wird durchgeführt, indem eine Antriebsmaschine an einen zweiten Motor angeschlossen wird, der das Drehmoment simuliert, das auf den Motor ausgeübt wird, während Öl an die Oberfläche gepumpt wird. Zusätzlich zu den Umrichter - Steuerungen, mit denen jeder Motor ausgestattet ist, musste eine Steuereinheit für den zweiten Motor eingeführt werden, um das charakteristische Drehmoment des Pumpsimulators anzuzeigen.

Ein wesentlicher Teil der Diplomarbeit besteht die Installation eines Messsystems, die Datenerfassungsphase und die für eine genaue Datenverarbeitung erforderlichen Mittel. Die Messungen der Prüfeinrichtung geben einen Einblick in die Leistung beider Motoren, indem sie Strom, Spannung, Drehmoment, Drehzahl und Position der Welle analysieren. Darüber hinaus gibt die Diplomarbeit einen detaillierteren Einblick in elektrische Verluste in bestimmten Betriebszuständen geben.

Der Teststand soll einen Einblick in die Kapazität und dass Potential der Asynchronmaschine vermitteln, indem ein bestimmtes Drehmomentszenario durch den Pumpensimulator bereitgestellt wird. Dadurch ermöglicht der Teststand die Identifizierung der Parameter, um einen Induktionsmotor zu einem energieeffizienteren Primärantrieb zu optimieren.

Acknowledgements

I would first of all like to thank my thesis advisor O. Univ.-Prof. Dipl.-Ing. Dr.Techn.Weiß Helmut who consistently advised me and guided me in the right direction during the thesis project. I would also like to express my gratitude to the experts who have been involved in the project's supervision and provided additional support to the research project:

- Dipl.-Ing. Winkler Thomas
- Dipl.-Ing. Dr.mont. Schmid Andreas
- Dipl.-Ing. Dipl.-Ing. Ziegerhofer Herbert
- Karsten Alexander

Their valuable insight and expertise has been vital for the outcome of this project.

Finally, I wish to express my very deepest gratitude to my family for providing me with continuous support and encouragement throughout my years of study. My achievements would have not been possible without their guidance and support.

Contents

Chapter 1 Introduction

Induction motors are commonly used as prime movers for powering sucker rod pumps in the oil and gas industry. The motive to write this thesis originated from the observation that in the field the prime mover of a sucker rod pumping system is often not adequately dimensioned. Prime movers are frequently consuming 8 to 10 times more power than an efficient pumping system in certain operational states. (M.A. Reedy, 2006) The high power demand is leading to an increase in operational cost and production wells might reach their economic limit earlier than planned. The prime mover can be powered by a generator or by the national power grid. Oversized induction motors can lead to additional strain on the power grid. Therefore, an adequate designed motor will lead to reduction in costs and minimize the impact on the national grid. The use of a test stand that offers an insight into the drive performance under real load conditions can represent a valuable tool.

The thesis discusses the methods used to design and construct a test stand to analyse an induction motor powering a sucker rod pump.

The prime mover which supplies the rotational energy to the reciprocating piston pumps, will be connected on the test stand directly to a second engine which counter acts the torque of the prime mover to recreate similar effects acting on the engine as during field operations. The second engine will be a sucker rod pump simulator. Both induction motors will be controlled with variable speed drives (VSD). Additionally, for conducting simulations and experiments on the two engines, a measurement system on current, voltage, power, torque and speed is required. Within this framework an analog circuit will be set up to program a signal that simulates an ideal torque against a time curve which will be reflected by the "pump-acting" engine.

Setting up the test stand will give insight into the motors capacity and potential by providing a specific torque scenario, therefore helping to optimize a more energy efficient prime mover. Furthermore, the thesis will also offer additional insight into electric losses during certain operational states.

The thesis will determine the necessary equipment with respect to drive hardware and measurement hardware including software for the project above mentioned and will guide through the development of the phases of the test bench to ultimately analyse the outcome of the test.

In the second chapter after the introduction the fundamentals which were the basis for creating the test stand are discussed. The fundaments do not only include the basics in electrical engineering but also give insight into the characteristics of the different kind of prime movers used in the industry. This chapter will also include a short summary on the functionality of the surface and subsurface structure of sucker rod pumping systems and the basis for selecting adequate prime movers for pumping operations.

In Chapter 3 the test stand design and used hardware are discussed. Furthermore, the motors and the VSD's which are used in the test stand are presented. Chapter 3 also

goes further and analyses the engines and VSD's works and how they have been modified to conduct experiments. The engine which is acting as a prime mover during the experiments is of a unique design known as a *Dahlander pole changing* motor. In this chapter the characteristics of this engine and their use in today's industry are discussed.

A central focus point of the thesis is the design and the calibration of the measurement system: the test stand is capable of determining the speed, torque, the power of the prime mover and the position of the shaft. The shaft positioning sensor puts the counter torque of the pump simulator in relation to the up and down stroke of a sucker rod pump.

In chapter 3, the design considerations and the difficulties of creating the sensors and data acquisition system are described in depth. Not only the sensor and data acquisition are explained but also the interface of all the sensors and the differential amplifier that had to be connected to the data processing card.

The measurement software is also described within the framework of the research together with an explanation on how the data had to be calibrated to receive reasonable results from the simulations.

The last section of chapter 3 is focused on the test stand control system. The chapter explains how the prime mover is speed controlled as it is usual in the industry to power a test stand and to program a pump simulator that is torque controlled. The thesis aims to recreate the characteristic torque curve from pumping operations by using a frequency generator as an input signal to the VSD of the pump simulator.

Chapter 4 describes in greater detail how the experiments have been conducted and analyses the outcome of these experiments. Four experiments have been done during the course of the thesis. More in specific, the constant load test, the short circuit test and an idling test were performed to understand the capabilities of the prime mover. Through these experiments the current locus was constructed and following this step the torque vs speed curve has been established allowing to determine how the engine can be classified. The final experiment is represented by the pumping simulation.

The aim of chapter 4 is to recreate not only the torque vs time curve of a sucker rod pump but also to link the shaft positioning sensor to the up and down stroke of the pump simulator. Additionally, the results of the pumping simulation have been compared to a real life field measurement from a sucker rod pump located in the area of Bocklfieß.

Chapter 2 Fundamentals

The following chapter describes the underlying fundamentals for sucker rod pumping systems.

2.1 Sucker Rod Pumping System

The sucker rod pumping system also known as beam pump provides the energy to lift hydrocarbons from the subsurface reservoir to the surface artificially. Beam pumps are standard in the Oil and Gas Industry since they are easy to operate and maintain in comparison to other lifting methods due to their relatively simple system design. Nevertheless a downside of the sucker rod pump is its loss in efficiency in gassy wells, its increased friction in deviated wells and an operating depth of only up to 4,3 km. (Economides)

2.1.1 Surface Structure

On the surface the beam pumping system consists of the prime mover, gear reducer, counterweights, crank arm, Pitman, walking beam, Sampson post, horse head, bridle, the polished rod, the stuffing box and the tee as seen in Figure 1.

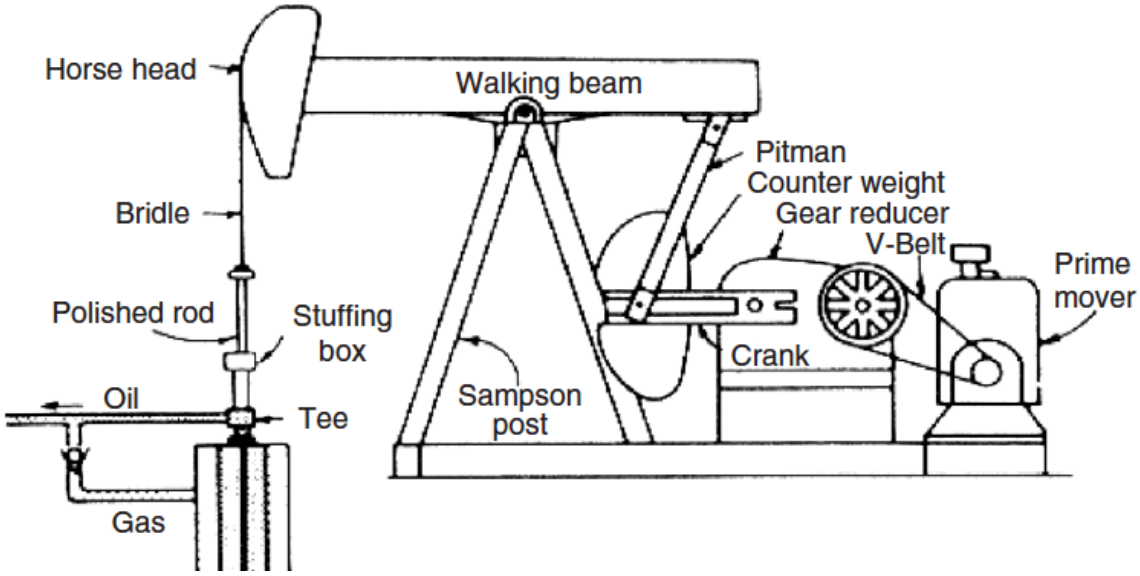

Figure 1 Surface Structure of a Sucker Rod Pump (Guo, Lyons, & Ghalambor, 2007)

The prime mover drives the gear reducer and it can be an electric engine or a combustion engine. The type of engine typically depends on the presence of a stable supply of electric energy for powering the prime mover, the required horsepower to pump the well, OPEX & CAPEX of the well and the availability of skilled personnel.

The prime mover rotates at a speed of 300 to 1200 revolutions per minute (rpm) which is then reduced by sheaves, V-belt drives and gear reducers to a pumping speed of 2 to 25 strokes per minute (SPM) (Lake & Clegg, Petroleum Engineering Handbook - Production Operations Engineering, 2007).The purpose of the V-belt is to transmit the energy from the prime mover to the gear reducer. The sheaves which are holding the V-belt are influencing the amount of SPM with their pitch diameter. The crank arm is connected to the gearbox and is rotated by the gear reducer and converts the rotational movement into an oscillatory movement. The counterweights which are meant to lower the power demand of the prime mover can be positioned at the end of the beam or of the crank arm. The counterweights can be adjusted by changing the load or the position along the crank arm or the beam to adjust the counterweight torque. The walking beam is meant to support the weight of the rods and the counterweights. The horsehead, on the other hand, is supporting the bridle and guarantees with its unique shape a vertical movement of the polished rod.

The wellhead assembly consists of the polished rod, the stuffing box, pumping tee, flowline, check valve, casing and tubing connection and pressure/temperature sensors (as seen in Figure 2).

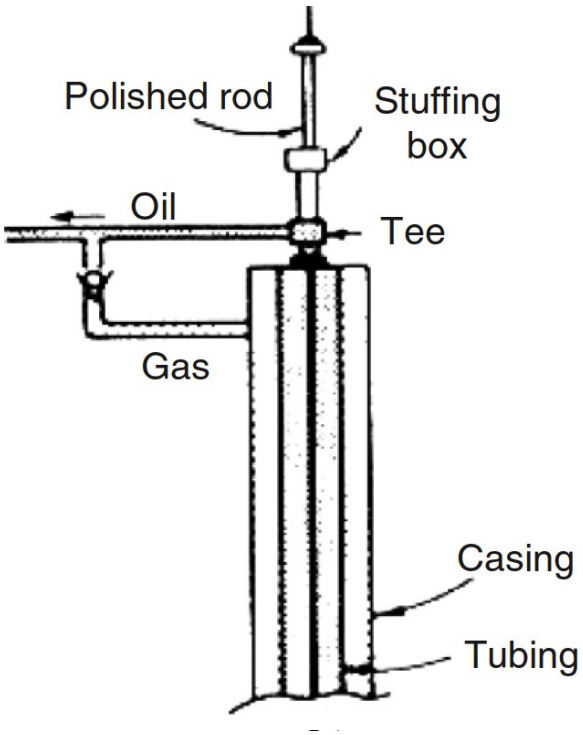

Figure 2 Wellhead assembly (Guo, Lyons, & Ghalambor, 2007)

The stuffing box not only allows a vertical movement but also provides a seal around the polished rod (that is connected by rod coupling to the rod string inside the tubing string).

2.1.2 Subsurface Structure

A standard pump consists of two valves with a movable plunger which is directly connected to the sucker rod string. There are two types of pump designs depending on how they are installed. The tubing pump is directly attached to the tubing, meanwhile the rod pump is inserted into the tubing (examples are shown in Figure 3).

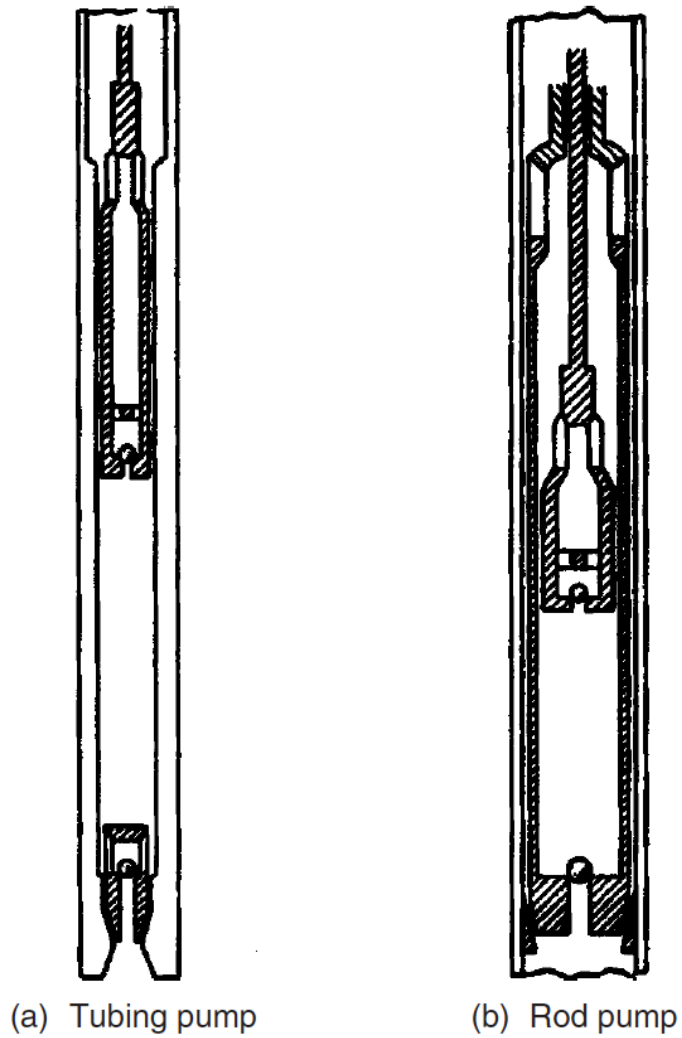

Figure 3 Types of pumps (Guo, Lyons, & Ghalambor, 2007)

When the rod string lifts the plunger during the upstroke, the travelling valve closes and the standing valve opens, thus allowing well fluid to enter the pump. During the downstroke instead, the travelling valve opens, and the standing valve closes so that the well fluid in the pump can enter the tubing. These steps can be seen in Figure 4.

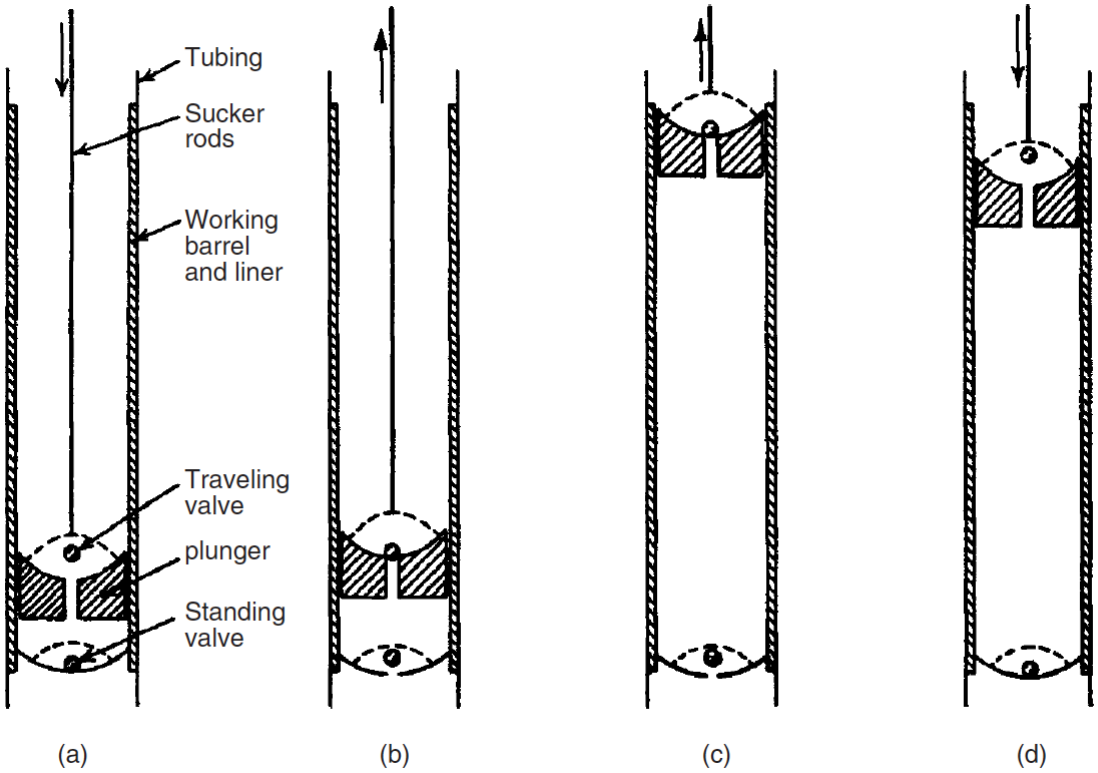

Figure 4 Sucker rod pumping illustration (Guo, Lyons, & Ghalambor, 2007)

2.1.3 Prime Mover

As previously mentioned either a combustion or an electric engine could power the pumping unit. The common electric engines for sucker rod pumping units are three phase squirrel cage induction motors. It is also possible to use single phase motors (up to 5 HP) if a three-phase engine is not available, but the cost of a single phase motor is considerably higher than a three phase motor for the same amount of power. (Lake & Clegg, Petroleum Engineering Handbook - Production Operations Engineering, 2007)

Table 1 shows the available engines corresponding to the voltages and sizes whose selection depends on the distribution-networks (Lake & Clegg, Petroleum Engineering Handbook - Production Operations Engineering, 2007).

	Up to 50 HP		**50 to 200 HP**
Engine	Single Phase motors	Polyphase motors	Polyphase motors
Required Voltage	115V, 230V	400V, 460V, 575V	400V, 460V, 575V, 660V, 796V

Table 1 General motor size vs. Voltage

The European Union classifies its engine according to the norm IEC 60034-30-1. This norm is grading engines according to their efficiency into four classes (Siemens, kein Datum):

- IE1 – Standard Efficiency
- IE2 – High Efficiency
- IE3 – Premium Efficiency
- IE4 – Super Premium Efficiency

In the US, on the other hand, the National Electrical Manufacturers Association (NEMA) has its own design standards. Graph 1 for instance, shows the different speed torque performances of the many NEMA design standards (Bishop, 2013).

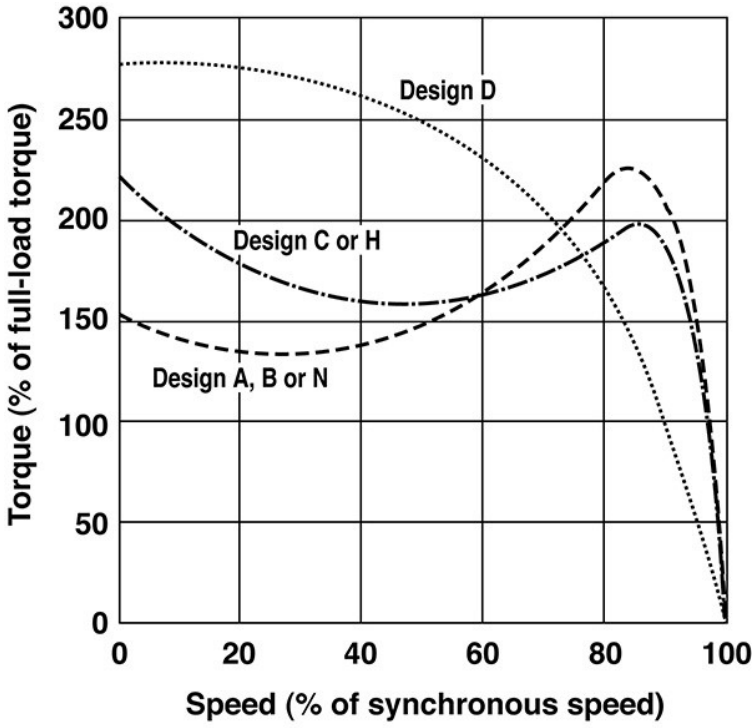

Graph 1 NEMA Design Standards (Bishop, 2013)

In the Oil and Gas Industry, the NEMA D engine with a synchronous speed of 1200 rpm is commonly used due to its high starting torque (as shown in Graph 1).

2.1.3.1 Characterisation of a Prime Mover

Essential elements for characterising prime movers are: current consumption I, useful motor power P_{out}, efficiency η, power factor cos φ, speed n, slip s and the torque M. Most of the information can be found directly on the motor nameplate, additional details can be calculated with the information contained in the nameplates and data sheets.

The power input of the motor P_{in} can be calculated by the formula below where U is the phase to phase voltage under which the motor is operating, I is the phase current and cos φ is the power factor.

$$P_{in} = \sqrt{3} * U * I * \cos\varphi \quad (1)$$

The mechanical Power P_{out} is calculated with Equation (2). The Power output is characterised by torque M multiplied by the rotational speed of the shaft.

$$P_{out} = M * \omega = M * n * 2 * \pi \quad (2)$$

The power loss of the engine is the difference of the power input and the power output - Equation (3). The efficiency of the engine is calculated by dividing the power output by the power input - Equation (4).

$$P_{loss} = P_{in} - P_{out} \quad (3)$$

$$\eta = \frac{P_{out}}{P_{in}} \quad (4)$$

The so-called electrical (complex) apparent power (S) of alternating currents is calculated via Equation (5). This can be split into active power (P) and reactive power (Q) as shown.

$$S = U * I^* = P + jQ \quad (5)$$

The active power is the mechanical power and heat dissipated of an asynchronous motor. The reactive power is created by the fact that the current is not in phase with the voltage due to different inductances and capacitances. When the current and voltage are in phase, the active power equals the apparent power and the reactive power is zero, see Graph 2 (left). If the current and the voltage are not in phase, see Graph 2 (right), active and reactive power can be calculated using equations(6) and (7) respectively.

$$P = U * I * cos\varphi \quad (6)$$

$$Q = U * I * sin\varphi \quad (7)$$

These relationships are shown in Graph 3 Power pointer diagram on the complex number plane.

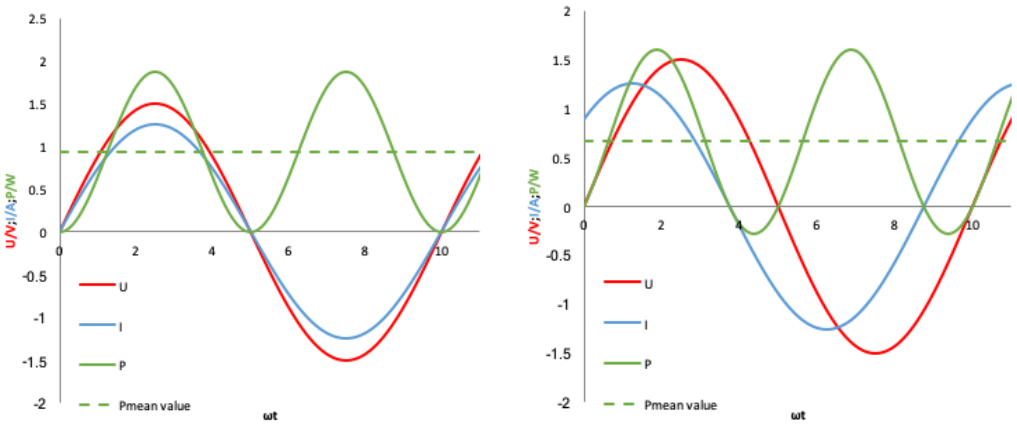

Graph 2 Power at I and U in-phase (left) and with phase shift (right)

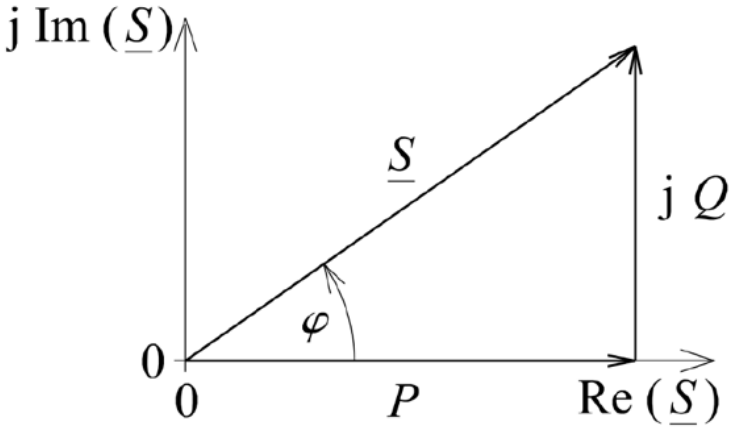

Graph 3 Power pointer diagram

The engine is selected by its nominal power which is calculated by Equation 8 where P_s is the polished rod power, f_c the cyclic load factor and η_m the mechanical load factor of the pump (Szilas, 1985).

$$P_{out} = \frac{P_s * f_c}{\eta_m} \tag{8}$$

The cyclic load factor is defined by the root mean square of the current which is proportional to the heating of the motor divided by the average current which is proportional to the useful output of the prime mover (see Equation (9)). The inverse of the Equation (9) is called the derating factor which is for NEMA D engines the value of 0,75 (Lake & Clegg, Petroleum Engineering Handbook - Production Operations Engineering, 2007).

$$f_c = \frac{\overline{I_{rms}}}{\overline{I_{avg}}} \tag{9}$$

Graph 4 represents different current consumptions within the up and down stroke (Lake & Clegg, Petroleum Engineering Handbook - Production Operations Engineering, 2007) versus the angular position of the engine with the resulting average current and root means square current.

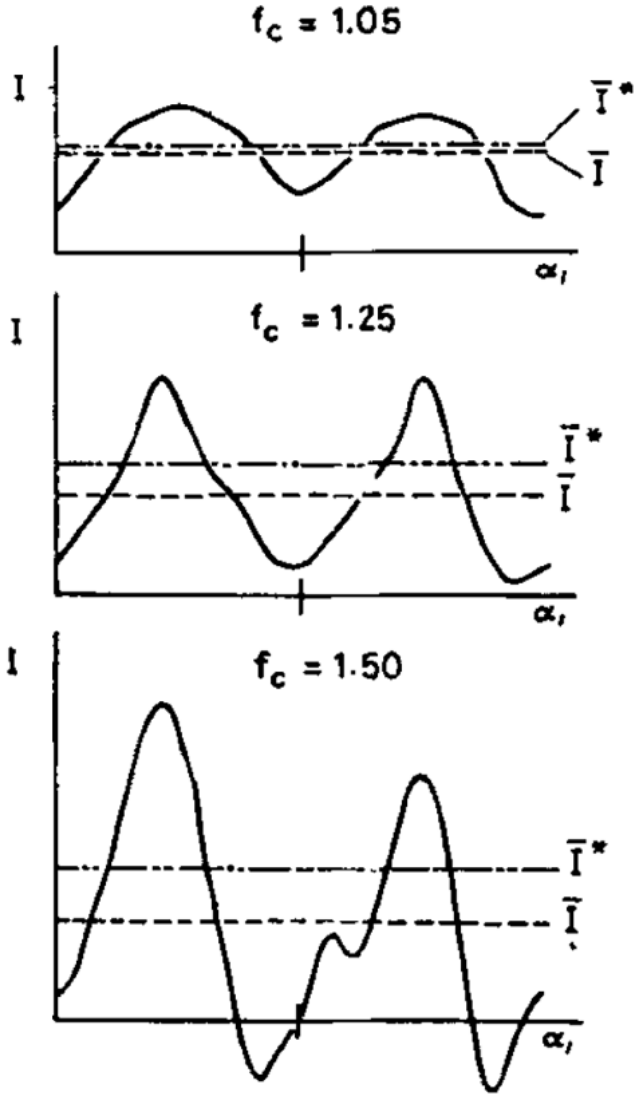

Graph 4 Current consumptions for different f_c within one stroke (Szilas, 1985)

The polished rod load is defined at the beginning of the upstroke with equation (10). Where $F_{dyn\,max}$ is the maximum dynamic polished rod load, it is comprised of the gravitational force of the fluid G_f and the rod string G_g. $F_{dyn\,max}$ is the force that has to be overcome to accelerate the polished rod. The Mills factor c is influenced by the length of the polished rod and the SPM.

$$F_{dyn\,max} = \left(G_g + G_f\right) * (1 + c) \tag{10}$$

At the end of the upstroke the velocity is 0, and the acceleration is at the maximum before the downstroke commences where the minimum dynamic polished rod load $F_{dyn\,min}$ applies (see Equation (11)). ρ_f is the density of the produced fluid and ρ_s is the density of the density of the sucker rods. (Langbauer, 2017)

$$F_{dyn\,min} = G_g * (1 - c\ - \frac{\rho_f}{\rho_s}) \tag{11}$$

The required polished rod power is calculated by integration of the Polished rod load multiplied by the velocity v(t) of the polished rod load (see Equation (12)). The velocity is dependent on the geometry of the surface unit.

$$P_s = \int_0^{\frac{T}{2}} F_{dyn}(t) * dv \tag{12}$$

The efficiency of the prime mover is calculated by Equation (13) where P_{in} is the electrical power intake of the prime mover.

$$\eta_e = \frac{P_s}{\eta_m * P_{in}} \tag{13}$$

To simplify the systems power requirement, equation (14) gives an estimation based on the fluid load G_f, the Mills factor c, the polished rod length h_p, the gravitational acceleration g, the SPM and the mechanical efficiency η_m.

$$P_{req} = 0{,}164 * G_f * (1 + c) * h_p * \frac{SPM}{g * \eta_m} \tag{14}$$

The power factor cos φ gives insight into how much line current is drawn by the prime mover. A low power factor below 0,80 (for NEMA D engines) can lead to penalties from the power companies since a low cos φ has higher line losses. (M.A. Reedy, 2006) This is likely to happen in the field since cos φ is load dependent and production wells have variable liftings throughout the life of the well.

The formula in Equation (15) is the slip of an induction motor. It is an indicator of how much torque can be converted by the prime mover, where n_s is the synchronous speed (or speed of rotating magnetic field) and n is the mechanical speed of the shaft. The synchronous speed is calculated by Equation (16) where f is the input frequency, and p is the number of pole-pairs. Since the frequency is in Hertz and the synchronous speed in rpm the formula needs to be multiplied by 60 to calculate the correct unit. With an increasing number of poles, the engine rotates slower. When the engine has only one pole pair it completes a full revolution within one period of the feeding frequency, if there are more pole pairs then the shaft rotates from one pole pair to the next, until the cycle is complete.

$$s = \frac{n_s - n}{n_s} * 100\% \tag{15}$$

$$n_s = \frac{60 * f}{p} \tag{16}$$

When operated as motor the speed of the shaft is slower than the speed of the rotating magnetic field in order to induce a current into the rotor.

The maximum rated torque of the engine is calulated at rated motor output power and the rated motor speed by the formula below. To obtain the torque in the Unit Nm it has to be multiplied by the factor of 9550 (with P_{out} kW and n RPM).

$$M = \frac{9550 * P_{out}}{n} \tag{17}$$

Chapter 3 Test Stand

The test stand under discussion is based on two engines having their own variable frequency drives (VFD). One induction motor acts as a prime mover (grey engine in Figure 5) and the second engine reflects the effects of the sucker rod pump on the prime mover (green engine in Figure 5).The test stand can evaluate the performance of the prime mover with the help of a counter torque given by the second motor (pump simulator). For the pump simulation, a signal is fed into the control system to simulate an ideal torque against time curve which is reflected by the "pump-acting" engine. For conducting simulations and experiments on the two engines, a measurement system on current, voltage, power, torque and speed is required. The test stand is to not only able to simulate specific scenarios to observe the prime mover's performance but also to test the engine in a controlled environment under field conditions. This chapter addresses the steps necessary to build the test stand and the measurement instruments.

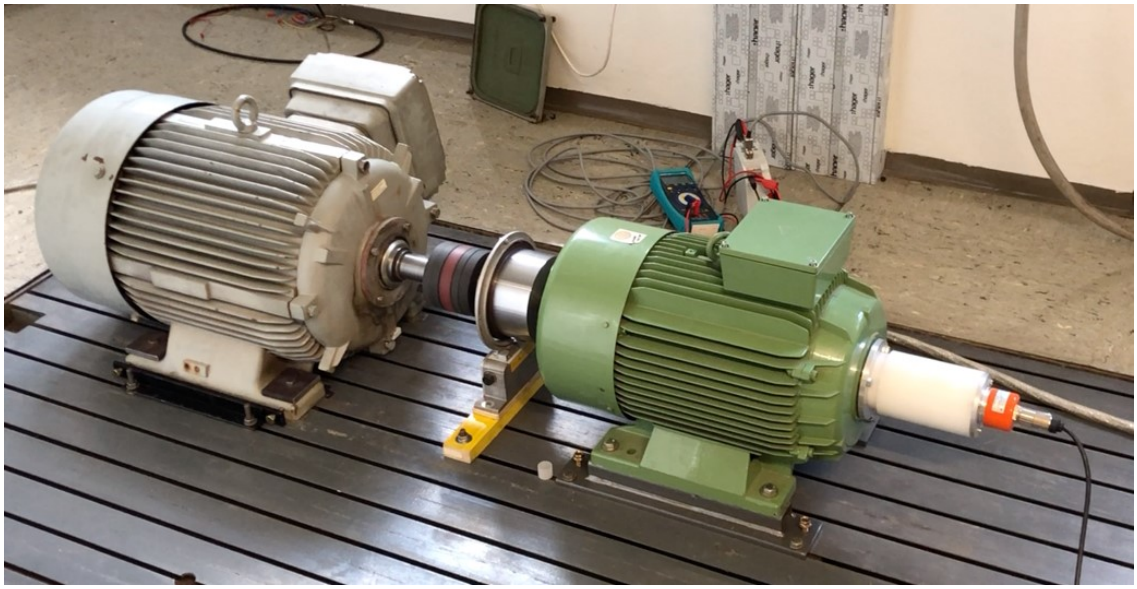

Figure 5 Engines of the test stand

3.1 Test Stand Components

The Test Stand consists of a VFD to control the prime mover. The prime mover is connected over a shaft with claw couplings to the motor of the pump simulator which generates the counter torque and is also controlled by a VFD. This set up is illustrated in Figure 6. The power supply for the VFD and the prime mover is coming from the power grid. The test stand is built as a closed system where the generated energy from the test stand (pump simulator) can be given back to the power grid. Therefore only the losses of the system (mainly both VSDs and machines) are obtained from the power grid.

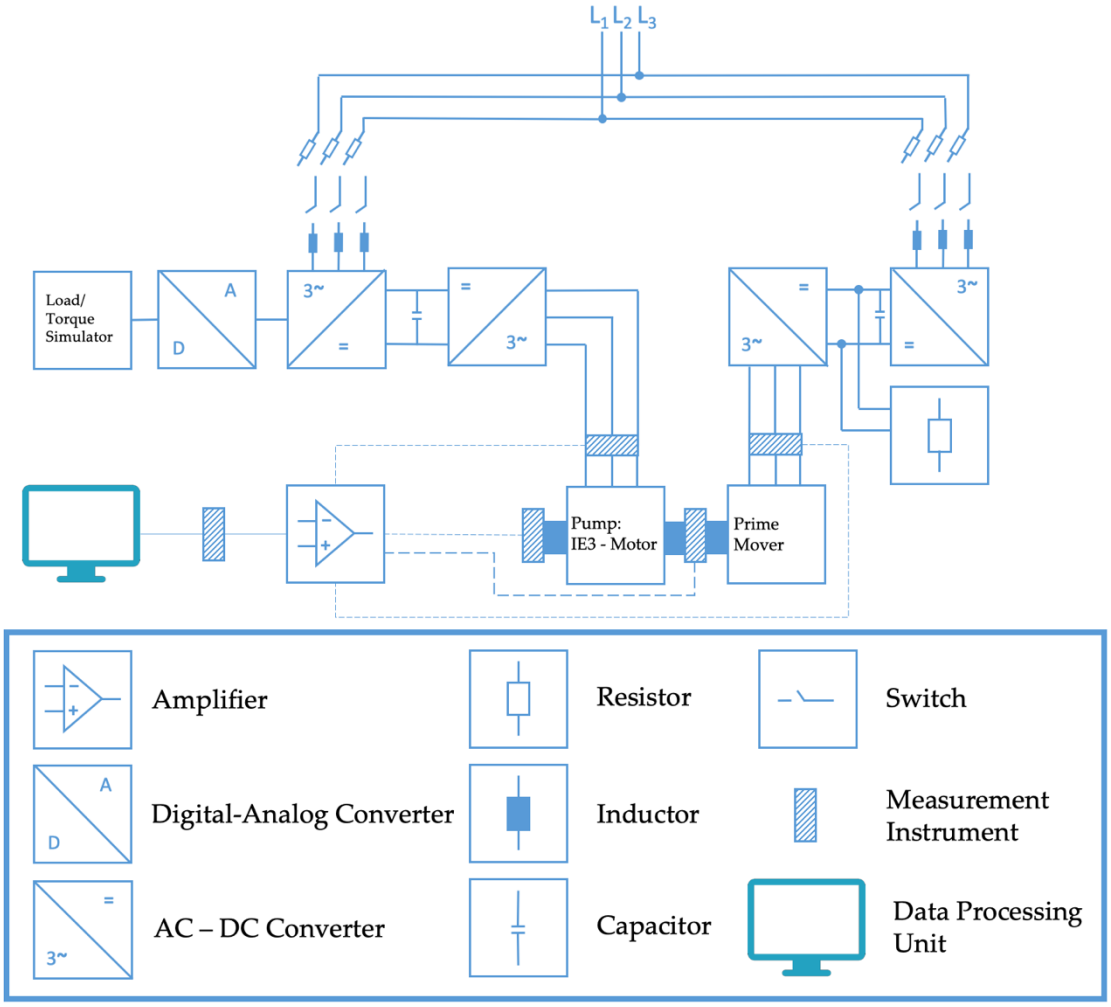

Figure 6 Experimental Test Stand set up

3.1.1 Dahlander Pole Changing Motor

The Dahlander Pole Changing Motor that can be seen in Figure 7 is the prime mover of the test stand. More in specific, the engine was provided by OMV Exportation & Production GmbH and was operational in the field until 2001.

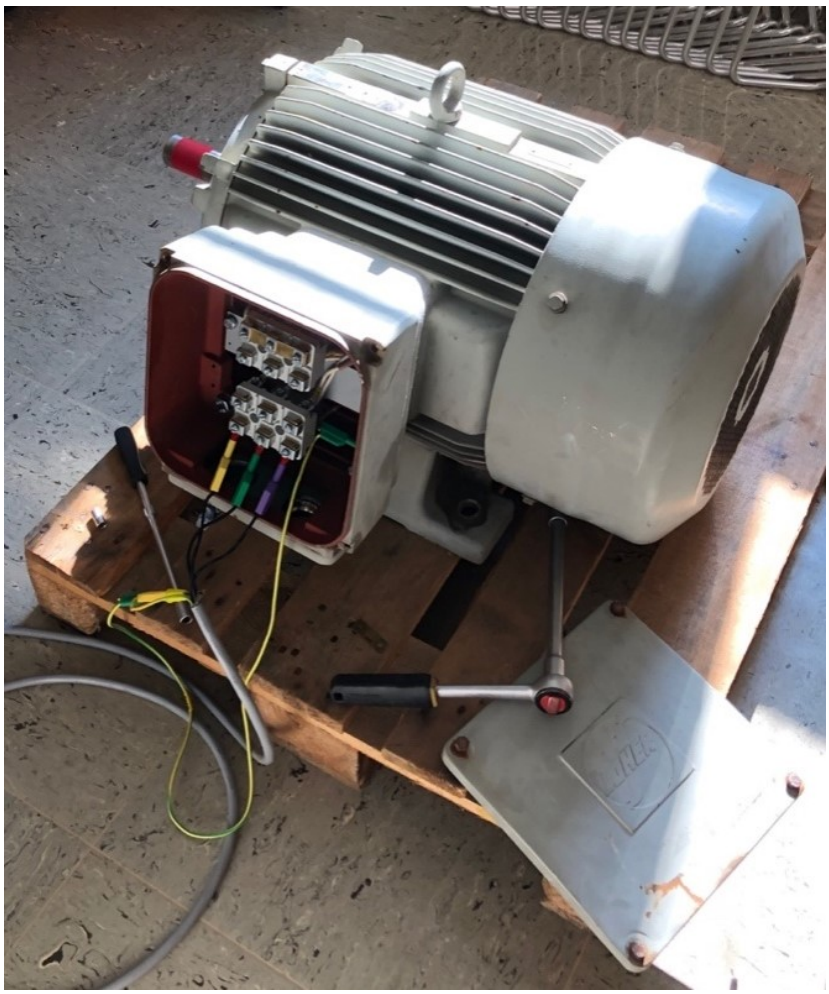

Figure 7 Dahlander Pole Changing motor

The motor is a 3-phase squirrel cage engine from the manufacturer Loher. Because it was used to power a sucker rod pump, it is equipped with Ex-protection. In Figure 7 the terminal where the engine is fitted with 9 ports (allowing star or delta connections for different speeds) can be seen. The speed of a beam pump can be adjusted either by changing the size of the sheaves or by changing the speed of the engine. The terminal in Figure 7 allows changing the speed the synchronous speed from a 735 rpm to 985 rpm and 1475 rpm. This kind of configuration in an engine is known as a Dahlander Pole Changing winding. The engine has 3 separate windings and the speed of the engine changes with the number of poles of the windings and with the supply frequency as it can be seen in Equation (16) (Toliyat & Kliman, 2004).

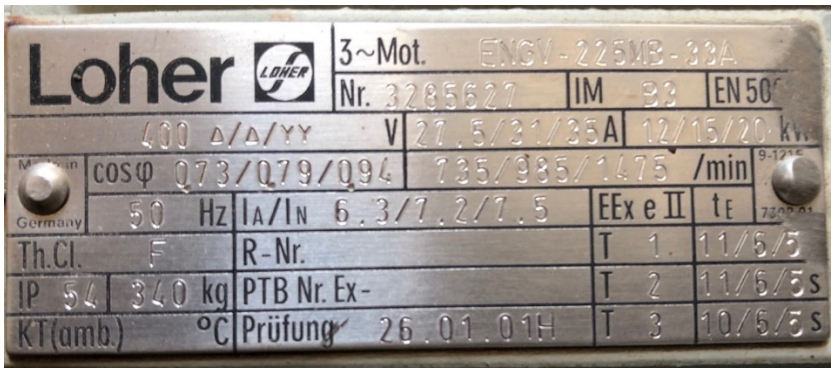

Figure 8 Prime Mover Motor Name Plate

From the type code on the motor nameplate, it is suggested that the engine has these pole pairs for each rated speed 8/6/4. The data plate also shows that the engine has a supply voltage of 400 Volts, a current consumption of 35 Ampere at full speed (for double star connection with a pole pair of 4 and a rated power of 20 kilowatts at full speed). The resulting power factor is 0,94 and the engine has an rpm of 1475 min^{-1}. Figure 9 shows how the interface has to be connected to get the desired rpm and power.

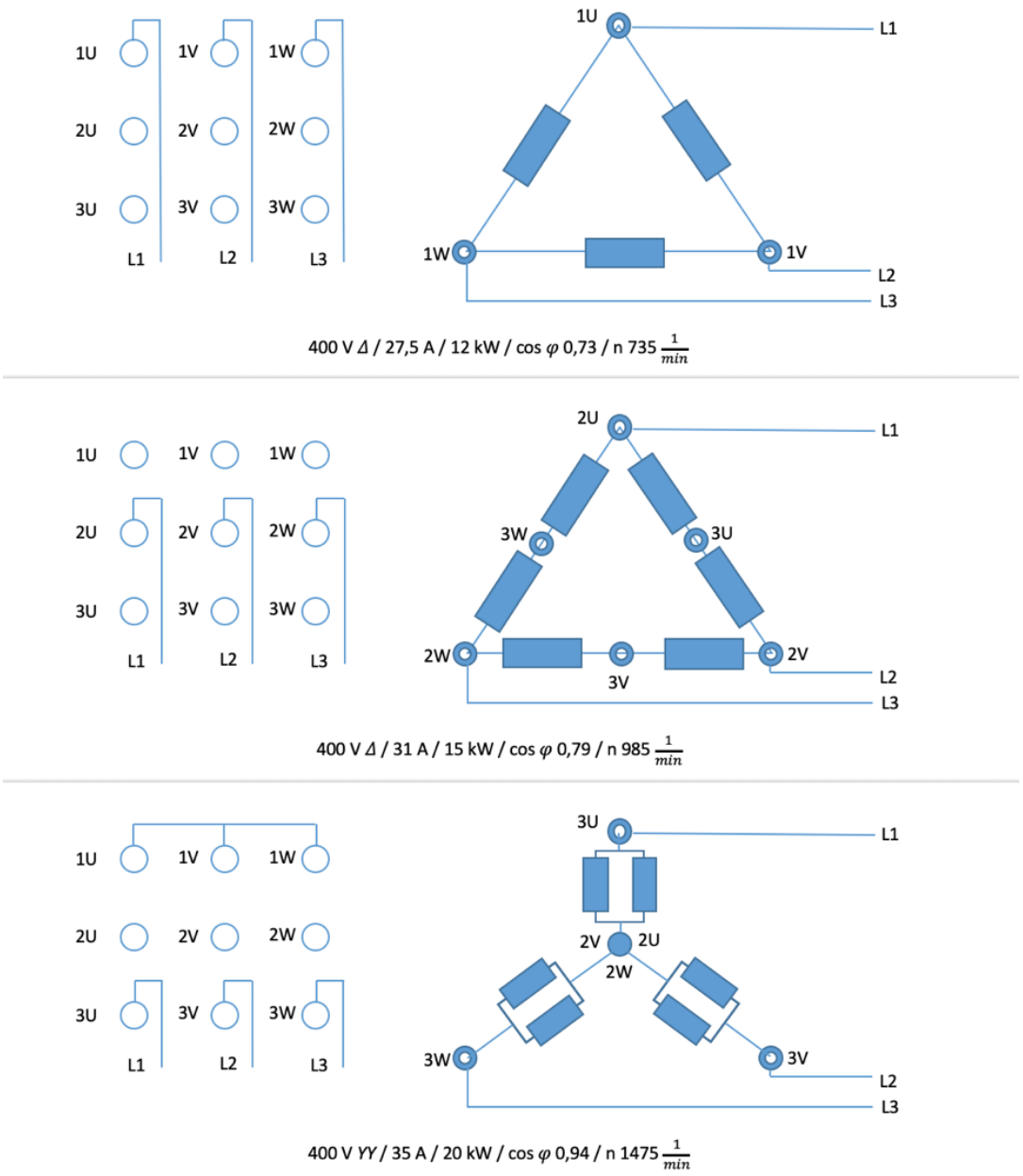

Figure 9 Dahlander Interface configuration

Other important values are not displayed on the nameplate of the motor and need to be calculated with the formulas mentioned in Chapter 2.1.3.1. The induction motor has a synchronous speed of 1500 rpm and a nominal slip of 1,67%. The power input of the engine is 22,8 kW and has a power loss of 2,8 kW. The efficiency of the engine is 88%. With the maximum rated speed and the maximum rated output power, the prime mover has a torque capacity of 129,5 Nm.

3.1.2 IE3 Motor

The pump simulator of the test stand is an IE3 3 phase industrial induction motor. The motor nameplate of the engine (Figure 10) shows that the engine has a power output of 22kW. The engine operates under a delta connection with a voltage of 380V, a current of 45 A and an input frequency of 50 Hz. The nominal rotor speed of the engine is 1460 rpm, and the power factor is 0,86. The engine serial number shows that the motor has a pole number of 4.

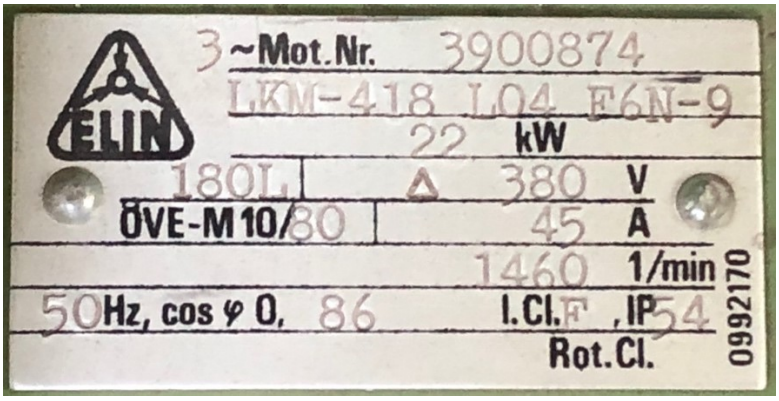

Figure 10 Pump Simulator Motor Name Plate

With the information from the motor nameplate, other factors can be calculated with the equations from Chapter 2.1.3.1 like the synchronous speed of the engine which is 1500 rpm. The motor has a slip of 2,67%. The electrical input power is 25,5 kW, and the power losses of the engine are 3,5kW. Therefore, the engine has an efficiency of 86%. It is also capable of a torque of 143,9 Nm. The motor also has the possibility to bolt an encoder on the back side of the engine, opposite of the shaft, as performed in this configuration as shown in Figure 11 (orange attachment).

Figure 11 Test Stand Pump Simulator

3.1.3 Variable Speed Drive

Through a frequency converter, also called inverter, the otherwise specified by the network frequency of 50 Hz can be changed arbitrarily to receive from the engine the same torque at different frequencies. This corresponds to a horizontal shift of the torque characteristic as shown in Graph 5.

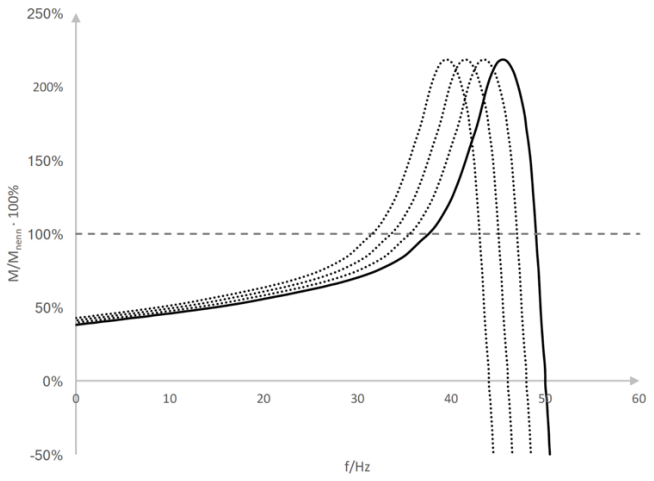

Graph 5 Effects of VSD drives on an induction motor

A frequency converter is a power converter that uses the fixed-frequency AC line voltage to generate a frequency and amplitude variable AC voltage for direct supply to electrical machines such as three-phase motors. Set points for frequency and amplitude of the AC output voltage depend on the requirements of the electrical machine and its current load. For this purpose, the three input voltages are converted through diode bridge rectifier into pulsating DC voltages, which are smoothed/filtered with capacitors and so supplying a conventional DC voltage intermediate circuit. Using Pulse Width Modulation (PWM), the desired AC voltage is generated from this DC voltage with at least six power semiconductors. This is shown schematically in Figure 12.

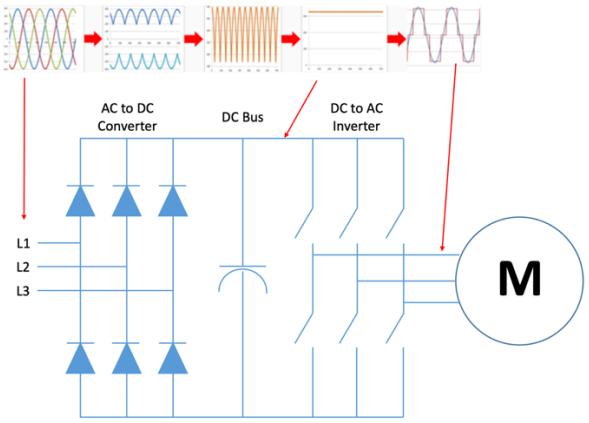

Figure 12 Working principal of a VSD drive (Harman, 2014)

3.1.3.1 SIMOVERT FC

The VSD SIMOVERT FC controls the prime mover of the test stand and is speed controlled (see Figure 13 right, blue rack).

Figure 13 VSD Drive SIMOVERT FC

The VSD SIMOVERT FC operates at a supply Voltage of 350 to 400 Volts with a supply frequency of 50 to 60 Hz. The VSD has a current demand of 61 Ampere for variable torque applications with an overcurrent of 136% of the rated current for 60 seconds. To the left, in Figure 13 a large resistor is illustrated. The reason why the VSD is equipped with a large resistor is to convert the breaking energy into heat when the prime mover is rotated by the pump simulator and is becoming a generator.

Modifications had to be made to use the VSD drive to control the prime mover. The built-in contactor Siemens 3TF43 for the SIMOVERT FC is not adequate for the test stand. The built-in contactor is rated for control of electric motors with 11,2 kW at 460

V. The contactor LC1D95B7 is used instead, as it is rated for motors with 33,6 kW at 400 V (see Figure 14 right).

Figure 14 Modifications to SIMOVERT FC

Additionally, for safety purposes NH00 fuses are added with a rated AC voltage of 500 V and a rated current of 80 A (Figure 14 middle).

3.1.3.2 SIMOVERT P

The VSD drive SIMOVERT P controls the pump simulator of the test stand and is torque controlled to simulate the pump (see Figure 15).

Figure 15 VSD Drive SIMOVERT P

The SIMOVERT P is capable of operating continuously on the AC supply Voltage in a range of 380 to 400 VAC with a supply frequency of 50 Hz. The output frequency, on the other hand, is in a range of 0 to 100 Hz and the output voltage is in a range of 0 to 400 VAC. The VSD drive is adequate for the pump simulator since the drive unit is capable of a current demand of 167 Ampere at 400 VAC with an overload capacity of 3/2 of the rated current for 60 seconds and has a rated power of 116 KVA. Also it is able to recuperate the breaking energy from the machine of the pump simulator (which is mainly working as a generator) back to the grid.

3.2 Test Stand Measurement Instruments and Senosrs

Chapter 3.2 discusses the measurement equipment used to investigate the test stand performance. The test stand is capable of measuring the voltage and current output of both engines. Additionally, it is also capable of measuring the rpm of the shaft and the torque it is exposed to.

3.2.1 RPM Sensor

To receive an accurate speed reading of the shaft on the test stand an incremental speed encoder has been attached to the pump simulator. The rpm sensor consists of a light emitting diode which acts as a transmitter and a photo-detector which is the receiver. A disk separates them with transparent sections. Pulses are being emitted by the encoder every time the photo-detector is activated by the light emitting diode when the transparent sections are passing by the diode. The output signal of the RPM sensor is characterized in pulses per revolution. The rotating disk has 3 tracks to identify the direction of rotation (see Figure 16).

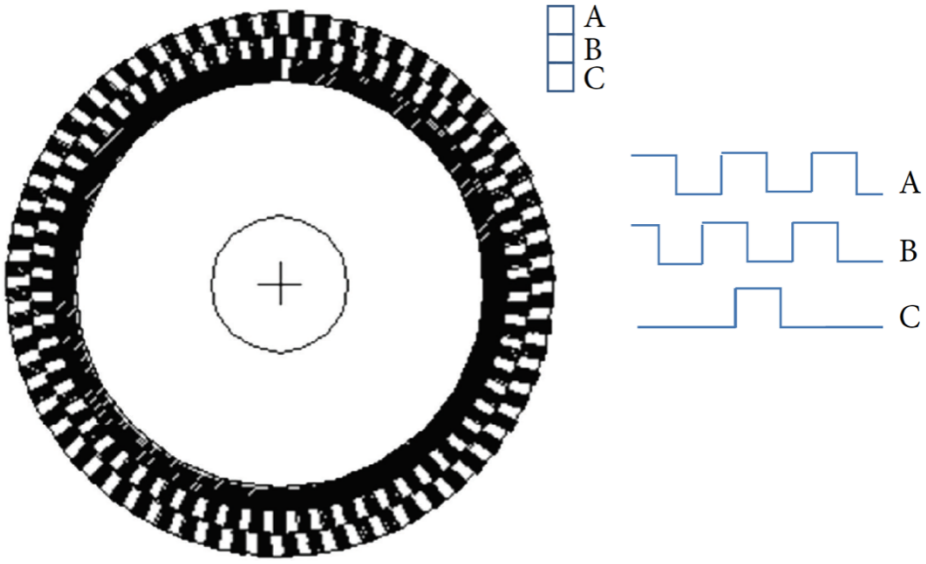

Figure 16 Speed Encoder Disk

Track B is 90° out of phase from track A thus if a pulse from track A is detected before the pulse from track B, the shaft is moving clockwise, and if the pulse from track B arrives before track A, then the shaft is rotating counter-clockwise. Track C also known as the reference signal indicates when a full revolution has been completed. The speed of the shaft is calculated with the formula below (Fiorucci, et al., 2013).The pulse rate of the encoder counts 1024 pulses per second, and the rpm sensor requires a supply voltage of 5 V.

$$RPM = \frac{Pulse\ Frequency * 60}{Pulse\ Rate} \tag{18}$$

An interface for the rpm sensor has been built to send the signal to the measurement system interface, to the VSD drive SIMOVERT P and the control unit of the pump

simulator. To protect the speed encoder, the control unit and other circuit boards connected to the VSD drive from voltage surges and to avoid a ground loop where two or more circuit systems have a different ground potential the circuit board has been galvanically isolated. This was achieved with an optoisolator which transfers electrical signals between two isolated systems by using a light emitter (diode) and a photo-detector. Figure 17 shows how the circuit board for the speed encoder interface was designed (left image), soldered on the back side of the circuit board (central image) and realised (right image).

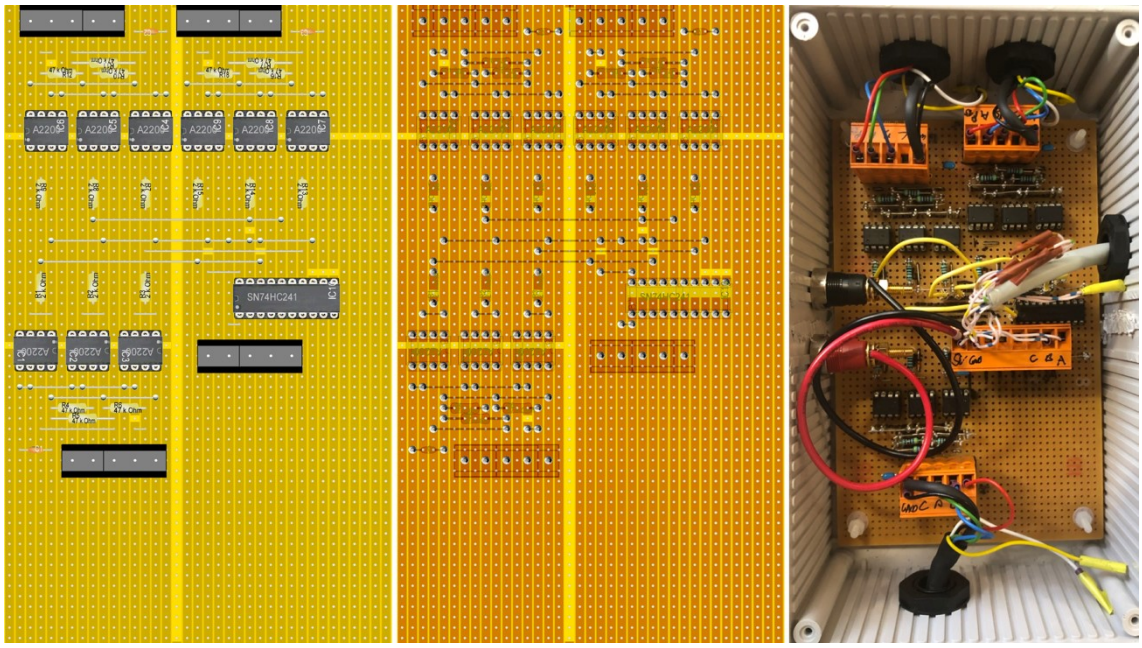

Figure 17 Circuit Board Design

For the interface optoisolators, type A2200 were built in, and a 2 kΩ resistor was installed at the input of the optoisolator to guarantee the necessary input current of 2,5 mA and the input voltage of 5 V. Since the input signal of the encoder interface has more than one output signal, more optoisolators are needed. This implicates that the required input current of 5 mA for each of the optoisolators is limited by the current capability of the output driver of the speed encoder. Thus an octal buffer was installed between the input signal and the optoisolators. Between the 15 V supply voltage of the optoisolator at the detector side and the output signal, a 47 kΩ resistor was built in to limit the output current to 25 mA.

To avoid programming the measurement software to convert the pulses from the incremental sensor into readable rpm a tachometer has been added to the speed measurement system (see Figure 18). For recording the speed, a Frequency-to-voltage converter has been developed in order to convert the frequency of the continuous square wave from on track into a proportional DC voltage. This voltage has to be scaled in the software to match the correct speed.

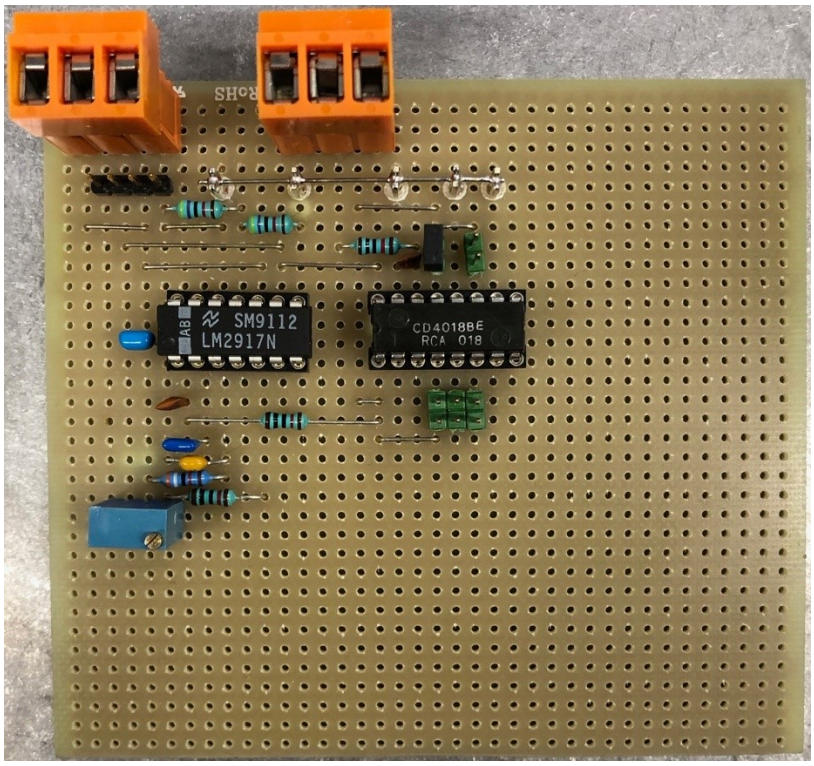

Figure 18 Tachometer

3.2.2 Shaft Positioning Signal

The shaft positioning sensor illustrates the up and down stroke of the pump simulator. The electronics input signal comes from the RPM sensor. The output signal of the shaft positioning sensor is a triangular signal. Each flank regardless if it is rising or falling represents one revolution of the crank arm. In order to prevent a counter overflow by the circuit board, the counter direction must be reversed after reaching the extreme values. Figure 19 shows the design of the shaft positioning sensor. An RS-Flipflop (1-bit memory circuit) obtains its input signal from a Wired-And respectively Wired-Or circuit. The RS-Flipflop was used to receive the output signals 11...11 and 00...00. This output signal is the result of the extreme values counting downwards or upwards to create the triangular signal.

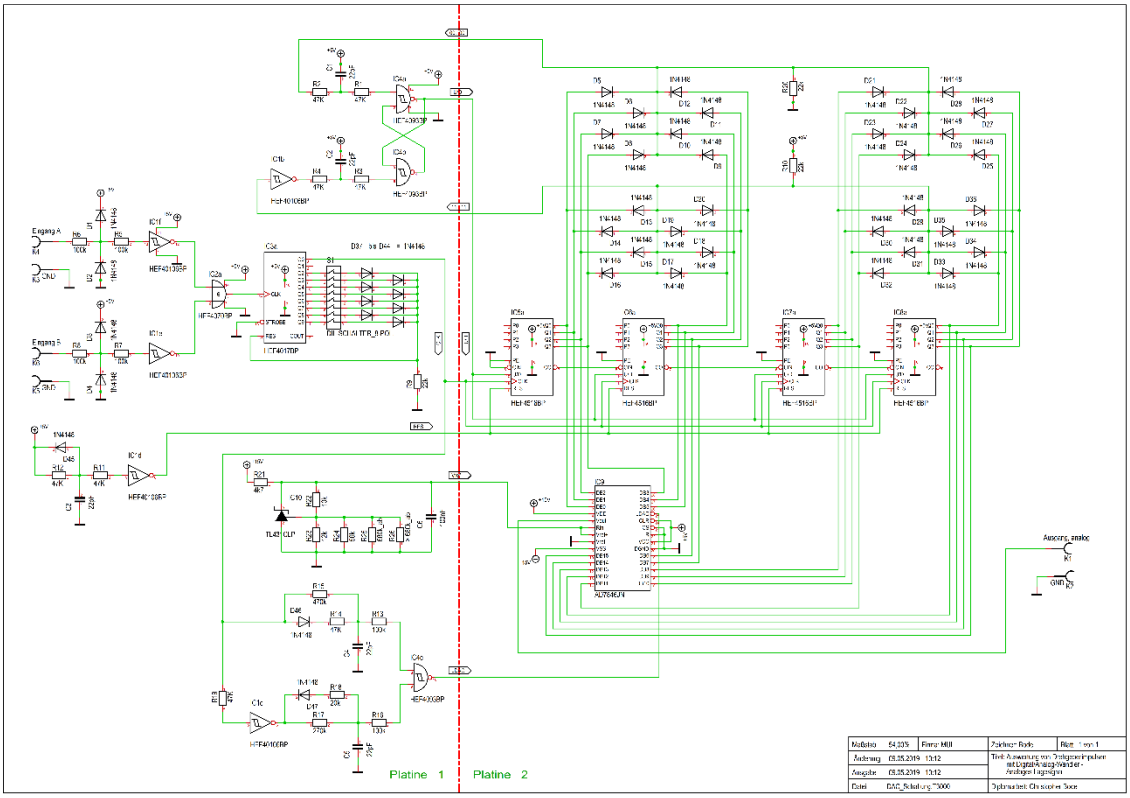

Figure 19 Shaft positioning sensor design

Track A and track B of the speed encoder (RPM sensor) produce each 1024 impulses per revolution of the shaft. The input signal is processed at the beginning through the inverter HEF40106BP. To improve the signal resolution both signals from track A and track B are linked together and doubled with the logic IC HEF4070BP known as an "exclusive-or".

The pulse number which is fed into the frequency counter equals the pulses from both tracks times the revolution per second (RPS) of the shaft. The shaft has a RPS of 25 and the number of pulses are 2048, therefore the input frequency into the counter is 51.200 Hz.

The IC HEF4017BP is a decimal counter which in this case is used as a frequency divider. Depending on the position of the DIP switch (also known as a mouse piano)

the frequency of the input signal can be divided into factors and will be passed on to the counter cascade.

In addition, a trigger signal is generated for the Digital Analogue Converter (DA) through the IC's HEF4093 (NAND) and the HEF40106 (inverter). Those are short impulses which are triggered while new data is being fed into the DA converter and exported. The handover signal is called LDAC.

After the frequency division, the clock signal (CLK) is passed on to a 16-bit counter pulse cascade. This consists of 4 times (HEF4516) 4 bit dual counters which are interconnected with a carry 16-bit counter. The status of the 16 output bits describes the rotation angle in binary data format. These bits are supplied to the DA converter as a parallel input signal. The output bits are evaluated with the above mentioned wired or a Wired-And to the extreme values. These signals are given back as 00 ... 00 or 11 ... 11.

The digital analogue converter receives its input data from the counter and the trigger signal. After each trigger from the trigger circuit, data is written on the analogue output as a value between minus 5 and plus 5 volts. An output filter is used to suppress fluctuations in the signal.

For the DA converter, a reference voltage of 5 volts is required this is generated by the TL431 reference voltage source, then stabilized and transferred to the DA converter.

Figure 20 shows the stripboard design of the shaft positioning sensor. Adjustments to the stripboard design and the circuit board design had to be made since the output signal showed too many disturbances.

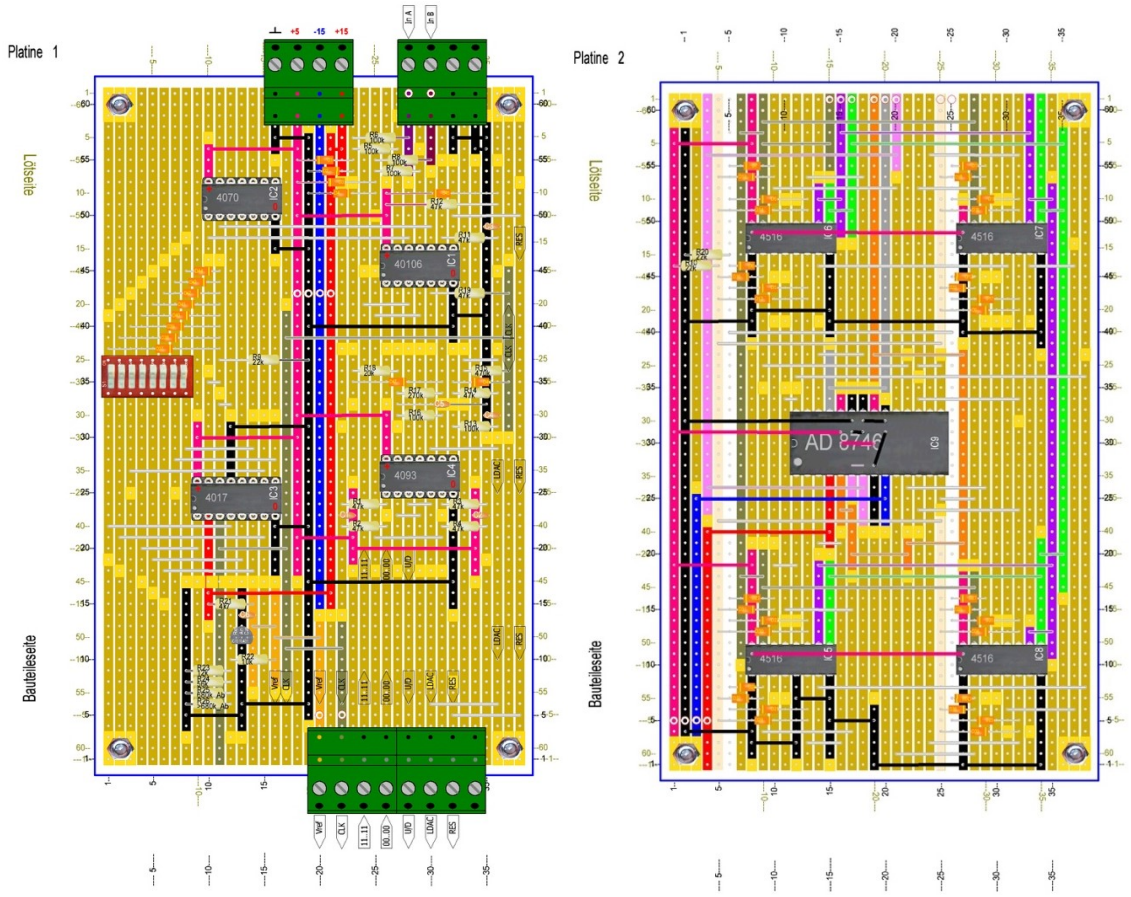

Figure 20 Shaft positioning sensor stripboard design

Unused pins of the IC's had to be relayed to ground to avoid disturbances from the microchip. These disturbances influenced the output signal and was observed on the oscilloscope in the range of 2,5 MHz. Another issue with the design was that too few capacitors were used to stabilise the voltage supply. 100nF capacitors were added to the voltage supply of the IC's and were added to the reference voltage. To avoid further interferences, the unused minus 5 Volt reference voltage of the IC's was relayed to ground. Also the DA converters power supply had to be stabilized with a 2,2 µF capacitor.

At the input signal the resistors were reduced due to the high self-capacitance of the 40106 inverter which led to a too high time constant of the E-function. Additionally the output signal was filtered with a low pass filter with 1 kΩ and 22 nF. Finally, the circuit board was placed into a metal containment for electromagnetic compatibility.

The most time consuming part in the construction of the circuit board was finding copper shafts on the stripboard and improper soldered components. These contaminations on the circuit board led to short circuits and interferences of the output signal.

3.2.3 Torque Sensor

The torque evaluation instrument used for the measurement system of the test stand is the torque flange T10F version SF1. It is installed on the shaft between the prime mover and the pump simulator with the claw couplings (see Figure 21). This system is not only capable of acquiring the torque which is applied to the shaft but also the rotational speed of the shaft itself. Since a speed encoder with a tachometer with a higher resolution is already in place (see Chapter 3.2.1) the use of the speed measurement option of the torque flange is obsolete.

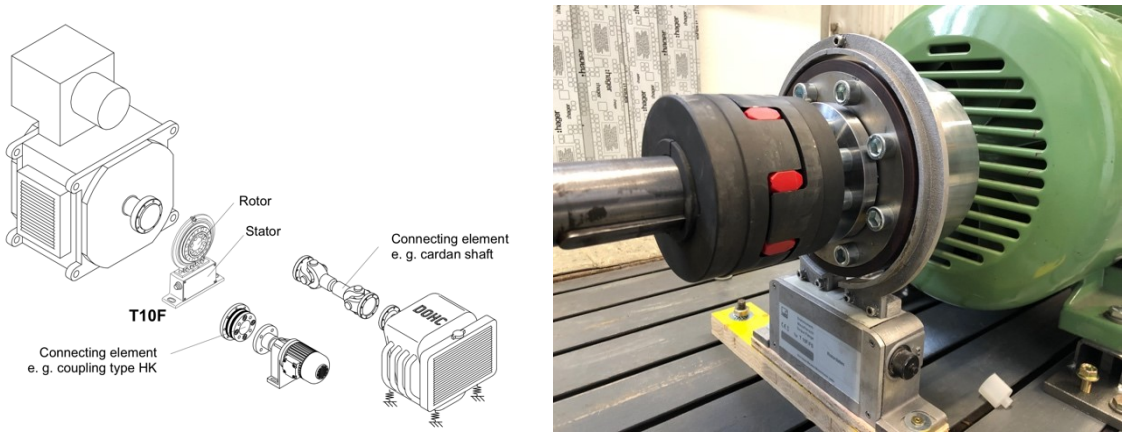

Figure 21 Torque sensor installation

The T10F torque flange records static and dynamic torque on a stationary or rotating shaft. The benefit of using the T10F is that it is incredibly compact, no bearing or slip rings, high permissible dynamic load and lateral forces and bending movements and has a very high torsional stiffness. Since the T10F uses no bearings, the measurement won't be influenced by friction and friction related heat transfers. Additionally, by not using bearings the voltage and measurement transmission is happening contact-free which results in no maintenance of the torque sensor. Therefore, it is essential to secure the measurement acquisition against electromagnetic interference. The measurement enclosure is acting as a Faraday cage, and the measurement cable is shielded from disturbances. Potential differences from test engine and the shaft can also influence the signal acquisition. This is avoided by connecting the shaft via wire loop and the stator to ground.

The torque sensor consists of the stator which is equipped with the power supply, the port for the measurement signal and the concentric antenna around the rotor. The movable rotor is equipped with four strain gauges mounted in equal distances from each other, transmitter coils for contactless power supply of the electronics and transmission of the torque signal. The rotor electronics is in the centre of the adapter flange and the transmitter coils are on the outer ring of the measuring body (see Figure 22).

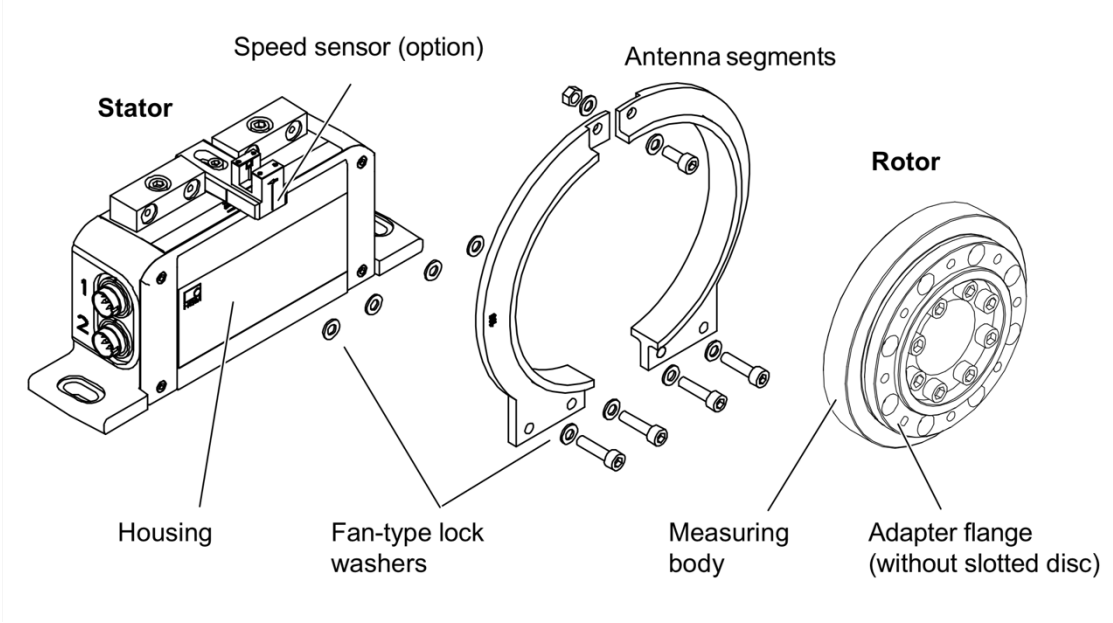

Figure 22 Mechanical build-up of torque sensor T10F (Hottinger Baldwin Messtechnik GmbH, 2018)

The calibration of the torque flange is done on the frequency measurement module MP60. It is crucial that during the calibrations sequence the rotor is not under any strain or stress. The calibration is done by the MP60 Module which measures the frequency at zero load and adjusts the measurement frequency with the calibration value from the identification plate of the torque flange. The torque sensor was tested by attaching a lever to the shaft at one side of the sensor and hanging known weights on the arm of the lever. Meanwhile the shaft at the other side of the sensor has been fixed. The frequency measurement module should display the predicted amount of torque which acts on the shaft by the lever. If the value displayed on the module deviates more than 1% from the predicted value, then the calibration of the test stand has to be redone since the T10F has an accuracy class of 0,1 (Hottinger Baldwin Messtechnik GmbH, 2018).

3.2.4 Voltage Transducer

Each engine is equipped with voltage transducers for electronic measurement of voltage for each phase. The used type is galvanic isolated between the primary circuit and the secondary circuit. Additionally, the voltage transducer is placed in a metallic box to avoid outside-disturbances during the measurement process (see Figure 23).

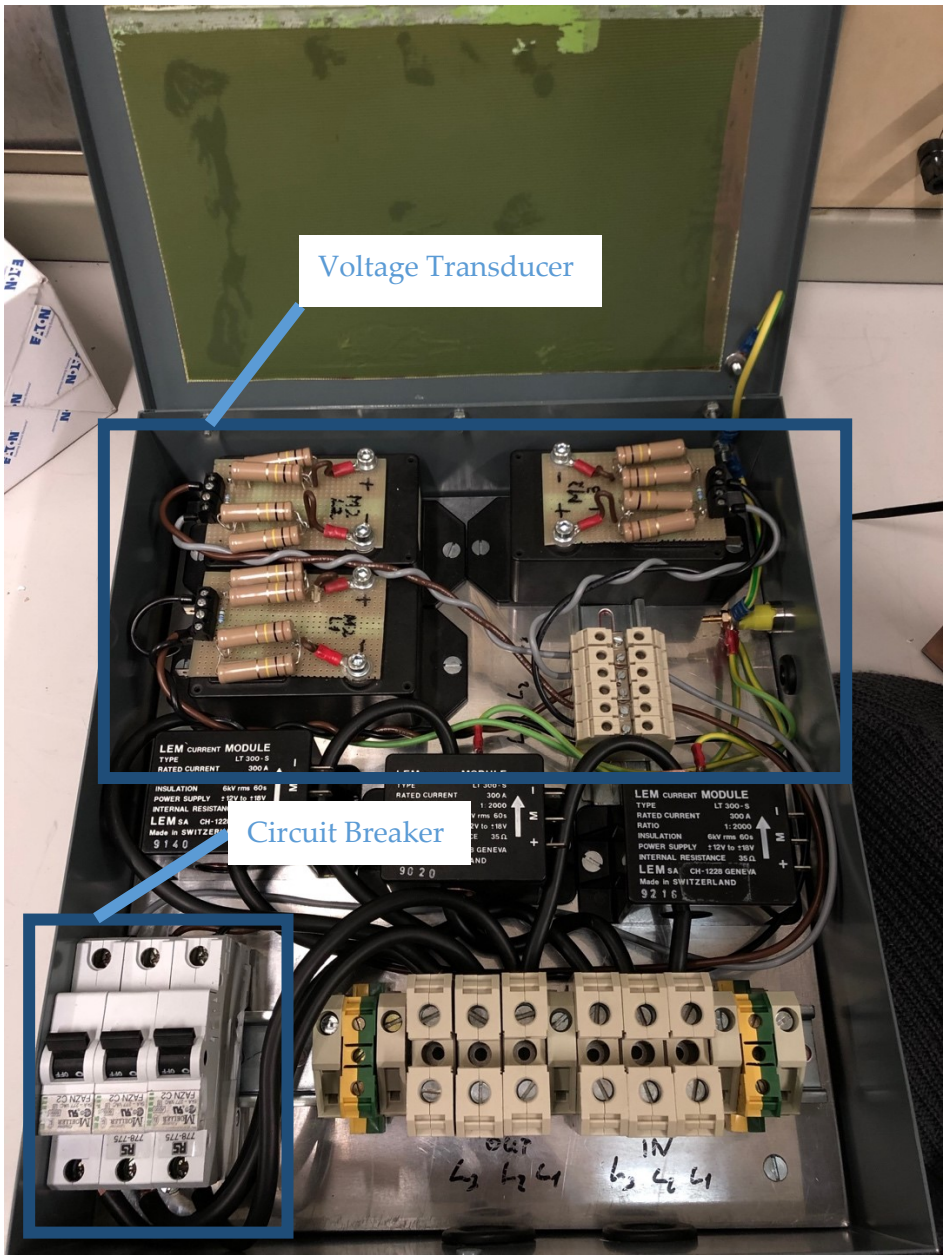

Figure 23 Voltage Transducer

The LEM Voltage Transducer LV 100 is designed for a primary nominal current I_{PN} of 10 mA in a range of primary nominal Voltage between 100 to 2500 V. The conversion ratio K_N of the transducer is 5:1, therefore the secondary nominal current I_{SP} is 50 mA (see Equation (19)).

$$I_{SP} = I_{PN} * K_N \tag{19}$$

A circuit board had to be mounted on top of the transducer to limit the sensing current to 10 mA which is drawn from the measured voltage. Even though the datasheet of the transducer says, the primary resistance R_P is 1900Ω, a Digital Ohm Meter was used to detect the exact internal resistance on the primary side for each transducer. The equation below was used to calculate the resistor R_1 on the primary coil.

$$R_1 = \frac{U}{I_{PN}} - R_P \tag{20}$$

The voltage transducer circuit diagram in Figure 24 shows that the transducer has a bipolar supply of ± 15 Volts. The diagram also shows that a sensing resistor R_m is necessary to convert the secondary current into a measurable voltage. For this experimental set up a sensing resistance of 200Ω was used.

Each phase is wired to a circuit breaker (bottom left corner in Figure 23) with a breaking capacity of 5 kA at 277 VAC. From the circuit breaker a twisted pair of wires (one for each phase) is connecting each voltage transducer to the phases. The first wire is going from the measured phase to the Terminal +HT and the second one is going from a different phase to the terminal –HT. It is important to connect the wire to the correct ports for calculating the phase voltage in the software. The sensing resistor has been built into the interface which gathers all of the measurement signals before passing through the differential amplifier.

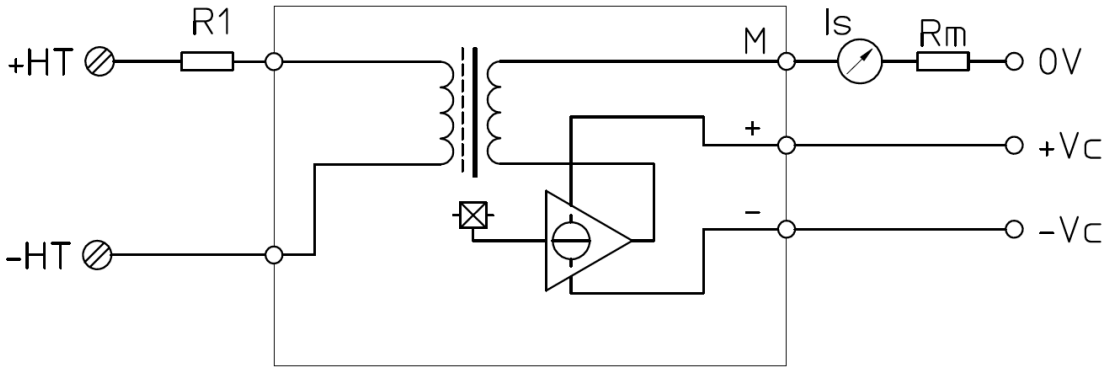

Figure 24 Voltage Transducer Circuit Diagram (LEM HOLDING SA, 2017)

3.2.5 Current Transducer

Additionally, to the voltage transducers, current transducers have been added to the measurement acquisition system (Figure 25).

Figure 25 Current Transducers

For measuring the currents of the prime mover, the LEM current Transducer LT 200-S was used and instead for the pump simulator the LEM Current Transducer LT 300-S/SP4 has been utilised. The difference between the two transducers is minimal. They only vary is in the current measurement range which is the same for both engines. The cable of the measured phase is passing through the magnetically permeable iron core to transform the magnetic field of the supply wire (primary circuit) to the secondary circuit. In the secondary circuit a controller/amplifier is compensating the field in the

core to zero by variegating the secondary current. Therefore a Hall Effect Sensor is placed at the core to measure the magnetic field (see Figure 26). The secondary current is transformed into a measurable Voltage with the resistor R_m of 200 Ω. The conversion ration K_N is 1:2000. The current transducer is galvanically isolated between the high power primary circuit and the secondary electronic circuit like the voltage transducer. A copper pipe has been fitted inside the current transducer and connected it to ground to avoid interferences with the measurement instruments.

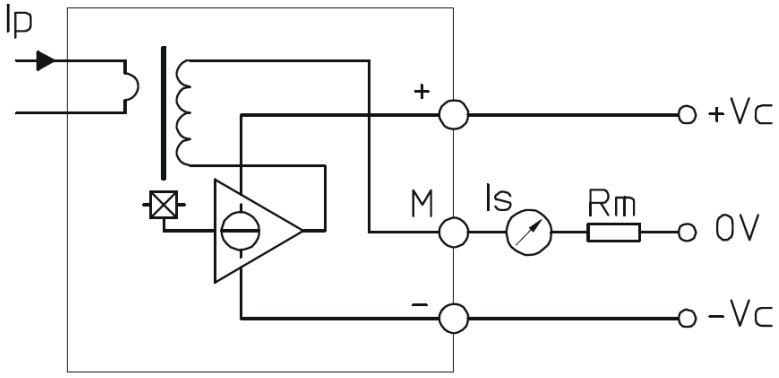

Figure 26 Current Transducer Circuit Diagram (LEM HOLDING SA, 2003)

3.2.6 Measurement Interface

All measurement signals are passing through the measurement interface (see Figure 27). All the cables which are passing from the measurement devices to the interface are equipped with a cable screen, and the interface is placed in a metallic box and connected to ground to avoid interferences during the measurement process. As mentioned in chapter 3.2.4 and 3.2.5 sensing resistors (R_m) are necessary to convert the current from the voltage and current transducers into a measurable voltage. In Figure 27 the high precision sensing resistors with a tolerance of 0,1% can be seen on the circuit board. The interface distributes the correct voltages to all the measurement instruments. The torque sensor has a power supply of 24 Volts. The voltage transducers, the current transducers and the tachometer have a power supply of +/-15 Volts. The supply connector for 24 Volts and 15 Volts bipolar can be seen in Figure 23 below. All the measurement signals are connected on the right-hand side of Figure 27 to a SUB-D 50 pin connector, to which the differential amplifier is connected.

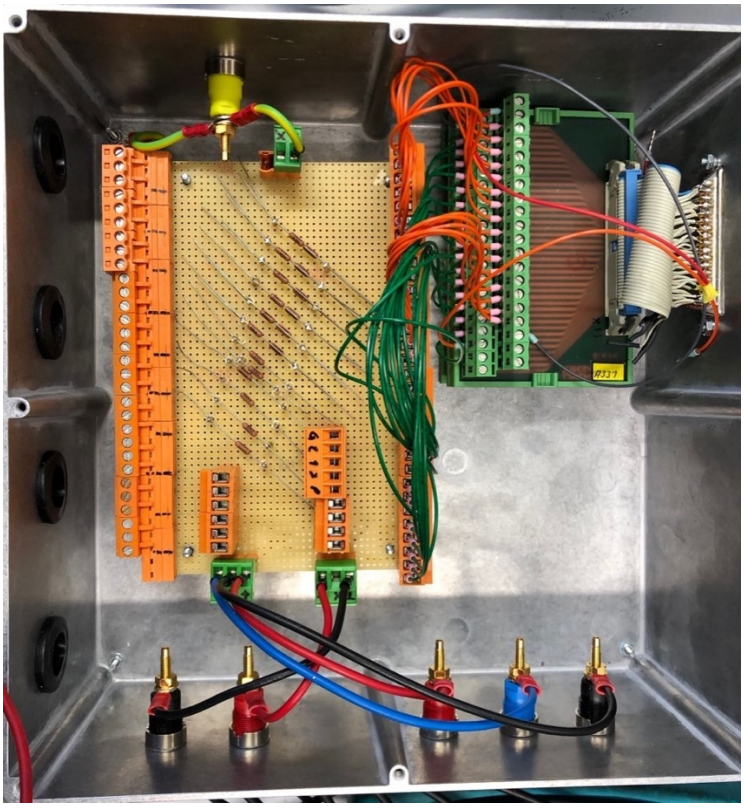

Figure 27 Measurement Interface

3.2.7 Differential Amplifier

To protect the measurement acquisition card in the data processing unit, the measurement system is equipped with an array of differential amplifiers which reduce the measured signals by a given factor. The differential amplifier amplifies the delta of an analogue signal by a factor determined by the resistors which have been built-in (see Figure 28).

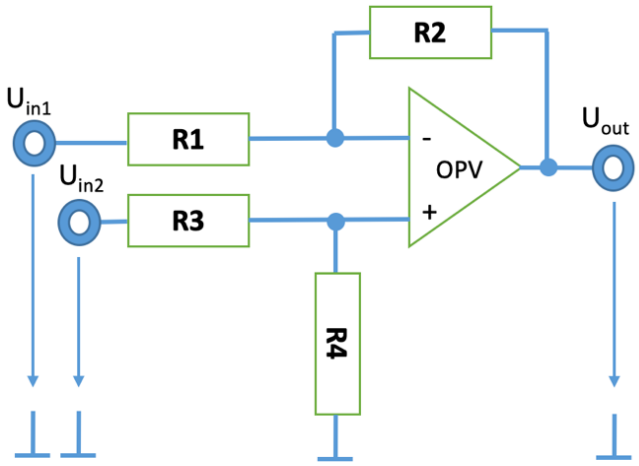

Figure 28 Differential Amplifier

If the input signal has to be inverted the signal U_{in1} is amplified by Equation (21) (U_{in2} to ground) and if a non-inverted signal is necessary the signal U_{in2} is amplified by Equation (22) (U_{in1} to ground).

$$U_{out} = -U_{in1} * \frac{R_2}{R_1} \tag{21}$$

$$U_{out} = \frac{R_1 + R_2}{R_1} * \frac{R_4}{R_3 + R_4} * U_{in2} \tag{22}$$

When using both inputs, the output signal is calculated by the following Equation (23).

$$U_{out} = \frac{R_1 + R_2}{R_1} * \frac{R_4}{R_3 + R_4} * U_{in2} - U_{in1} * \frac{R_2}{R_1} \tag{23}$$

Simplified with $R_1 = R_3$ and $R_2 = R_4$ the following Equation (24) is the result.

$$U_{out} = \frac{R_2}{R_1} * (U_{in2} - U_{in1}) \tag{24}$$

High capacity loads at the amplifier are leading to instabilities of the output signal. To avoid the amplifier to have any capacity load by the incoming signal cable or any display devices the signal at the inverted and non-inverted input needs to be decoupled. The cable at the inverted and non-inverted input needs to be a twisted pair to avoid any capacity loads. Additionally, large resistors before the signal enters the amplifier aid in the reduction of these effects. In Figure 29 Diodes are clamped to

conduct overvoltages or undervoltages to the amplifier supply (up to the designated supply voltage) (Weiß, 2018).

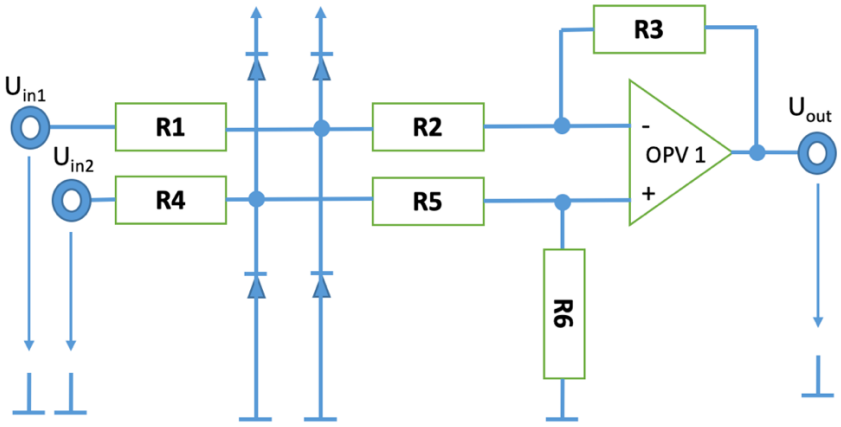

Figure 29 Amplifier high Voltage protection

As previously mentioned not only the incoming signal cable but also imaging devices like an Oscilloscope have capacitive loads that influence the signal stability depending on how high the capacity load is. Since the frequency of the channel sampling rate is high enough the Signal acquisition is not affected by a low pass filter (Figure 30).

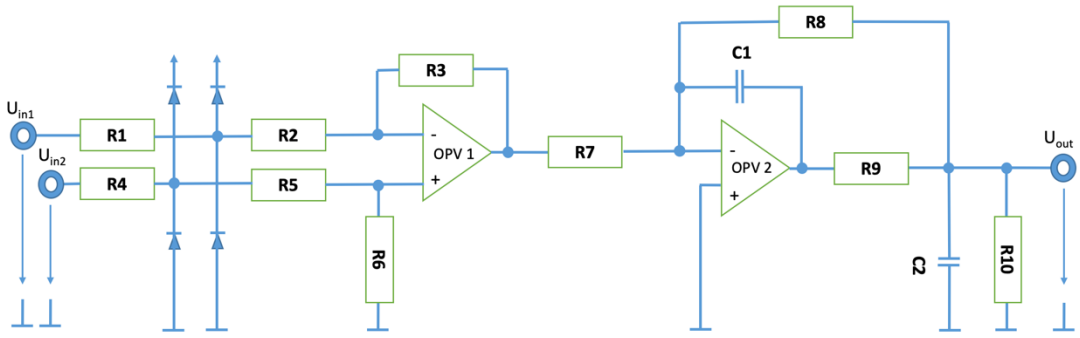

Figure 30 Differential Amplifier with Low Pass Filter

To reduce the incoming signal by a factor 0,5 the resistors R_1 to R_6 have 100 kΩ to decouple the incoming signals. The resistors of the low pass filter R_7 and R_8 have a value of 1,2 kΩ, R_9 has 270 Ω and R_{10} has 10 kΩ. The capacitor C_1 has 1,5 nF, and C_2 has 3,3 nF. The amplifier of the test stand consists of two circuit boards that combined have 32 signal inputs and 16 analogue outputs. The amplifier has been placed in a metal box to avoid interferences during the measurement acquisition phase. The design on the circuit board and the soldered result can be seen in Figure 32.

For the differential amplifier and other measurement components of the test stand ground loops are necessary not only for safety but also for maintaining the quality of

the signal acquisition phase. Because of the interference caused by compensating currents which is leading to potential differences it is of the essence to decouple the supply voltage ground and the housing ground. Figure 31 shows how the signal quality is improved by connecting the test stand measurement system to the same ground.

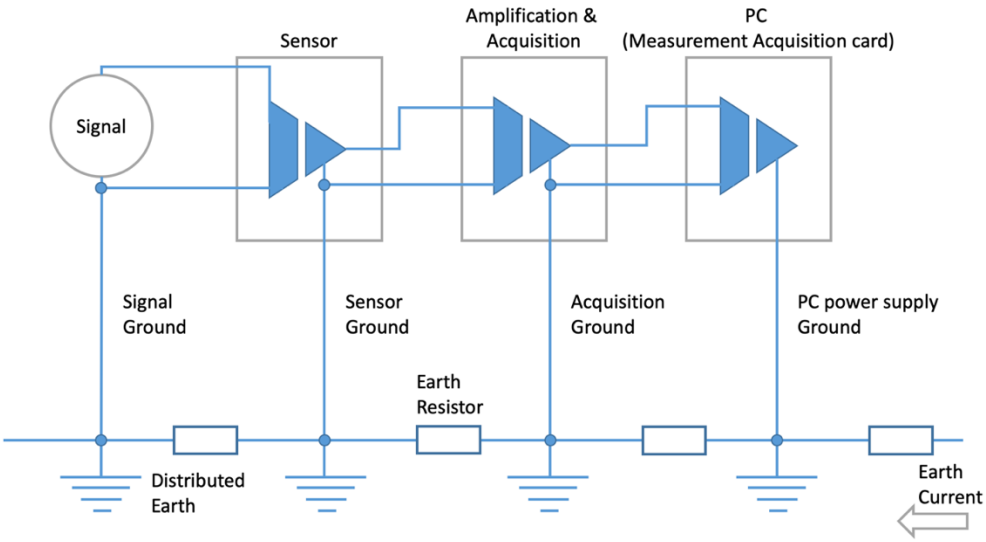

Figure 31 Potential Separation

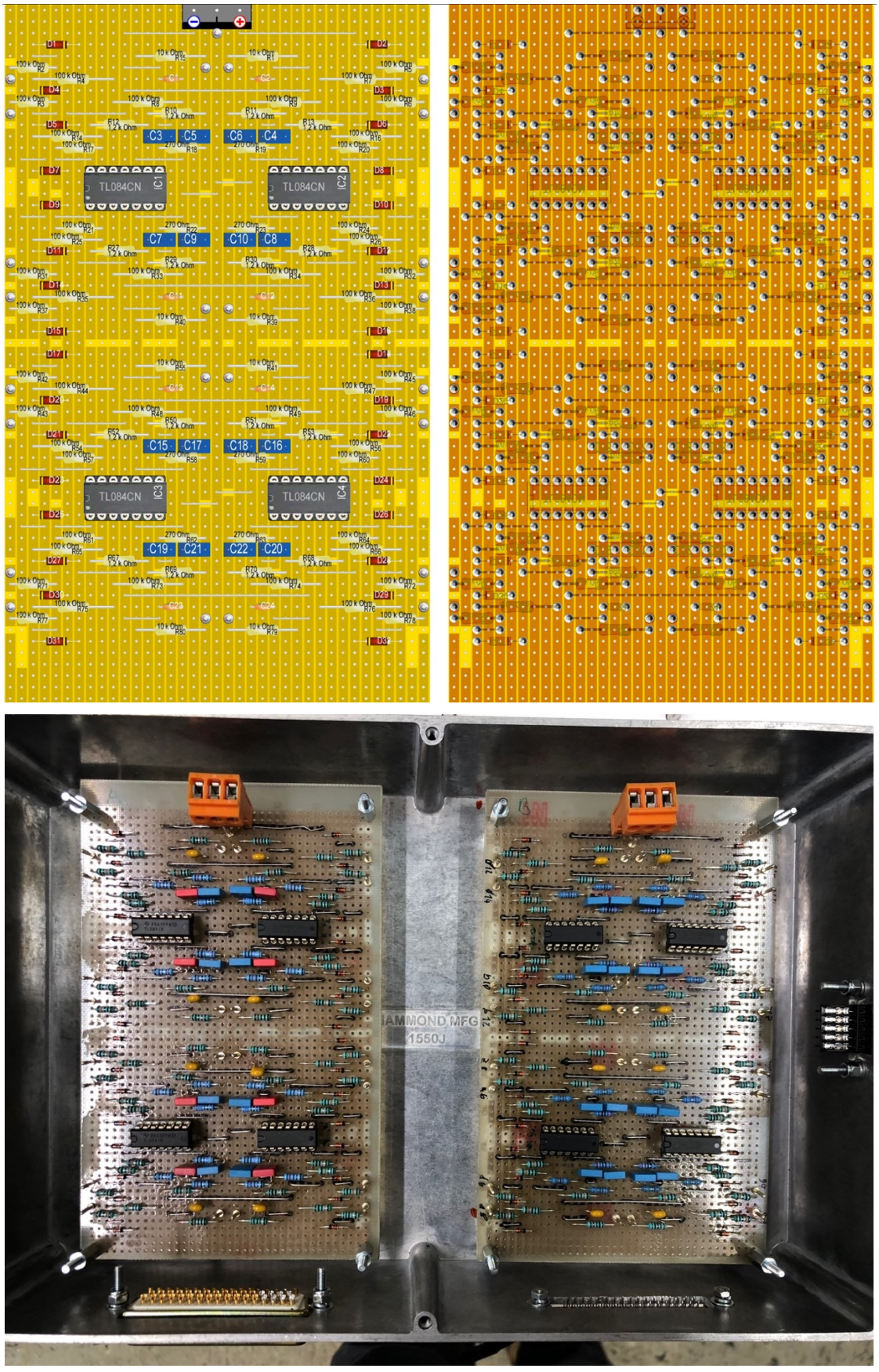

Figure 32 Differential Amplifier Circuit Board design front side (left) and back side (right) and soldered result (bottom)

3.2.8 Data Acquisition & Processing

The measurement acquisition card NI6220 is used to process the data on the computer. The measurement acquisition card has 16 analogue inputs which are connected to the differential amplifier after it has been established there is no short circuit from the incoming signals of the test stand. The acquisition card has a measuring range up to 10 Volts and a voltage protection up to 25 Volts.

The software which is used to interoperate the signal is DEWESoft7. This software is used to analyse and present scientific data. The measurement output from the differential amplifier is given in voltage and needs to be put in perspective.

In the channel set up in the software the analogue inputs are identified and assigned according to measurement performed. In the setup menu the measurement range, scale and Unit can be changed to the correct signal characteristics. The channel set up also allows to select the sampling rate. This is an essential factor to consider because if there are too low sampling rates, aliasing effects may influence the results interpretation and if the sampling rates are instead too high, the disk space on the hard drive may be compromised. For this experimental set up a sampling rate of 5000 Hz per channel has been selected.

To correctly calibre the current measurement in the software a known current of 40 Amp is sent through the test stand. Through the current transducers, the current is reduced to 20 mA. In the measurement interface of the test stand the measurement resistors produce a Voltage up to 2 Volts and are decreased down to 1 Volt through the differential amplifiers. Due to the age of the components and the ambient temperature analogue errors like offset and gain errors need to be corrected in the software. Graph 6 shows the ideal reference voltage which should be displayed by the software and the total error due to the offset and the gain. The effects cannot be seen well in Graph 6 since the total error deviates slightly from the reference signal.

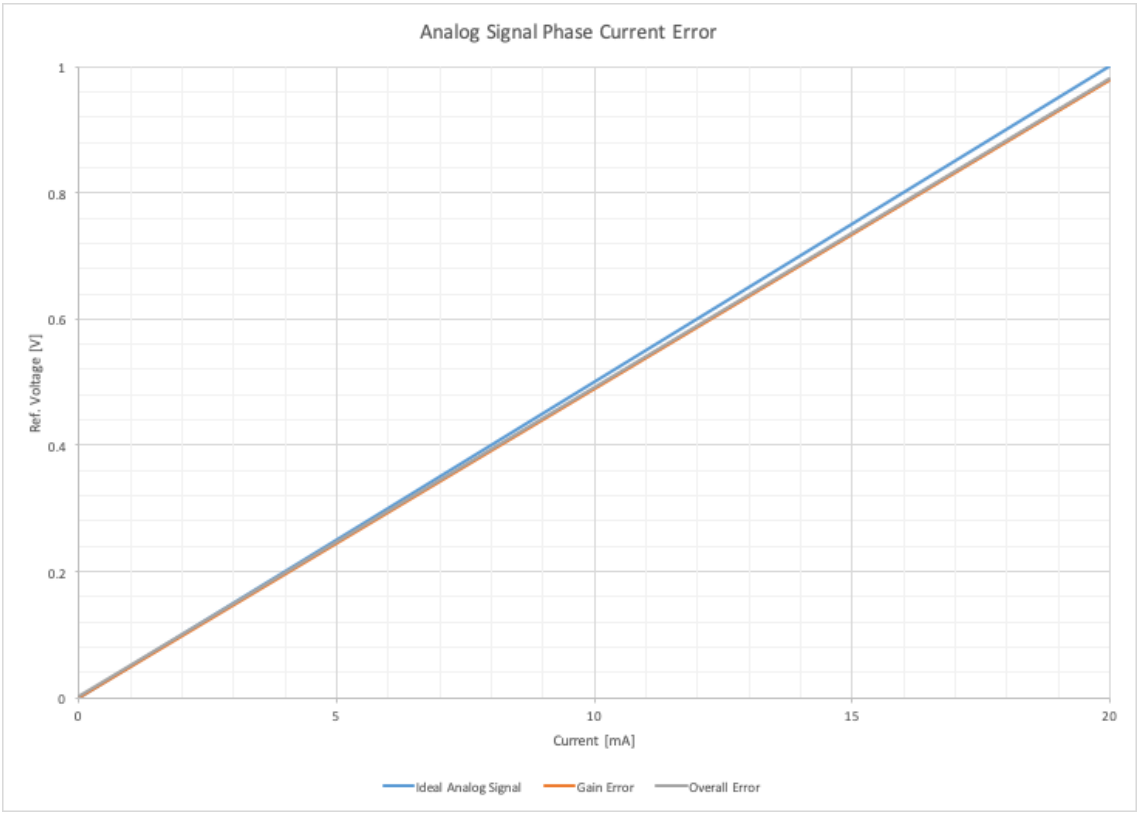

Graph 6 Analogue Signal Error

These effects are mitigated through the software by applying the formula below where k is the scaling factor, U_{in} the incoming Voltage, n the Offset and U_{ref} the reference Voltage.

$$U_{ref} = k * U_{in} + n \tag{24}$$

Finally, to correctly display the measured results in the software the reference Voltage for the current measurement needs to be scaled by a factor of 40 and displayed in Amps (see Figure 33).

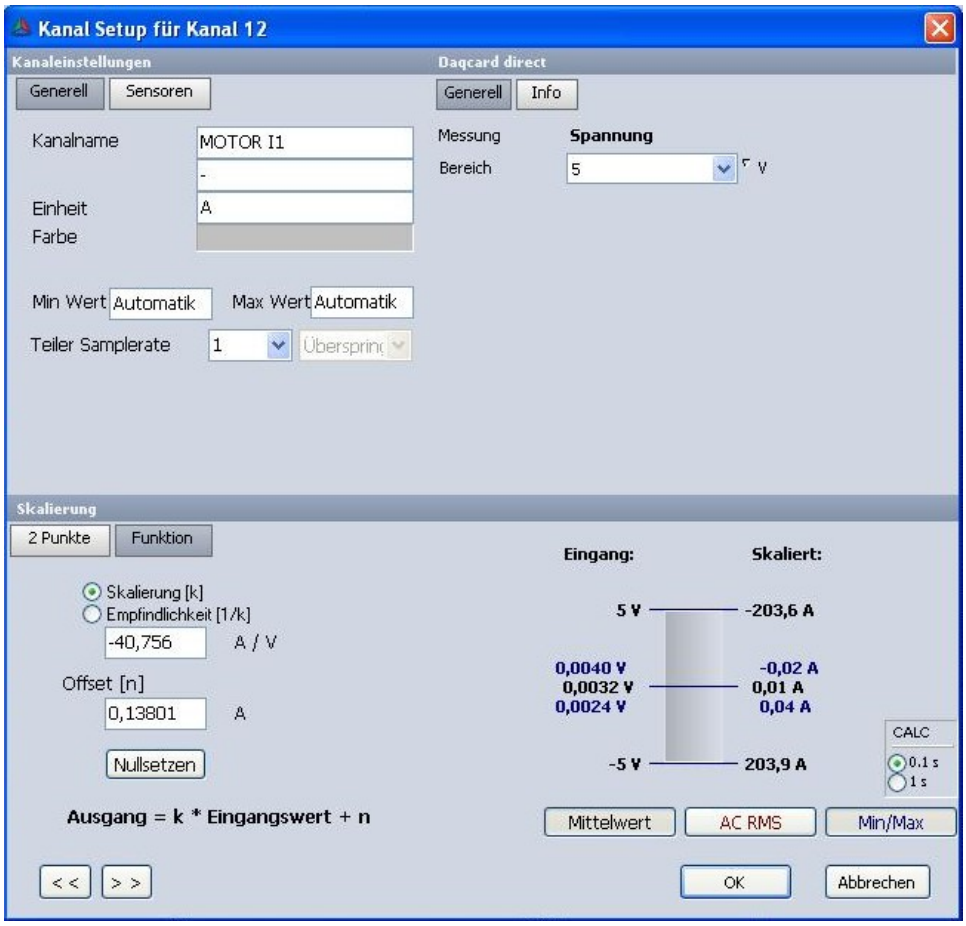

Figure 33 Signal calibration

The same procedure has to be done for each investigated analogue signal. The Table below shows the scaling factors which are used for every analogue signal.

Measured Signal	Analogue Input	Measurement Output Unit	Offset	Scaling Factor
Prime Mover Phase Current 1	AI12	[A]	1,38E-01	-40,76
Prime Mover Phase Current 2	AI13	[A]	1,46E-01	-40,80
Prime Mover Phase Current 3	AI14	[A]	2,67E-01	-40,86
Pump Simulator Phase Current 1	AI15	[A]	-1,40E-01	-40,57
Pump Simulator Phase Current 2	AI8	[A]	-4,46E-02	-40,82
Pump Simulator Phase Current 3	AI9	[A]	6,75E-02	-40,76
Prime Mover Line Voltage 1	AI0	[V]	1,45E-00	202,98
Prime Mover Line Voltage 2	AI11	[V]	1,17E-00	201,49
Prime Mover Line Voltage 3	AI4	[V]	6,50E-01	202,80
Pump Simulator Line Voltage 1	AI5	[V]	5,01E-01	193,69
Pump Simulator Line Voltage 2	AI6	[U]	1,43E-00	191,61
Pump Simulator Line Voltage 3	AI7	[V]	-8,49E-02	194,04
Speedometer	AI10	[rpm]	-4,32E-00	600,23
Torque	AI3	[Nm]	1,34E-01	100
Shaft positioning angle	AI1	[°]		
Not assigned	AI2	[-]	[-]	[-]

Table 2 Software gain and offset error mitigation

Table 2 shows that the scaling factors for the current for each engine and each phase are negative the reason for this is that the current transducers connection ports are inversed which can be easily corrected with the software.

The software has the possibility to customise formulas with the incoming analogue signals to display characteristic features of the testing stand. For instance, the momentary power of the engine was displayed by multiplying the current signal with the voltage signal of each phase (see Equation (25)).

$$P_m = U_1 * I_1 + U_2 * I_2 + U_3 * I_3 \tag{25}$$

But to calculate the momentary power the phase voltage needs to be calculated for each phase since the voltage transducers are only measuring the line-to-line voltage regardless of Δ or Y connection. The phase voltage is calculated by creating an artificial neutral point with the equations below.

$$U_1 = (U_{12} - U_{31}) * \frac{1}{3} \tag{26}$$

$$U_2 = (U_{23} - U_{12}) * \frac{1}{3} \tag{27}$$

$$U_3 = (U_{31} - U_{23}) * \frac{1}{3} \tag{28}$$

The software package also offers filters and statistical analysis of the signal. This is necessary to calculate the active power by applying the average function to the momentary power. The apparent power of the engine is calculated by multiplying the effective current (root mean square of phase current) with the effective voltage (root mean square of phase voltage) of each phase (see Equation (29)).

$$S = I_{1\,rms} * U_{1\,rms} + I_{2\,rms} * U_{2\,rms} + I_{3\,rms} * U_{3\,rms} \tag{29}$$

The root mean square of the investigated signal (phase current or phase voltage) needs a low pass Butterworth filter since the unfiltered signal has many fluctuations due to the inverters (see Figure 34).

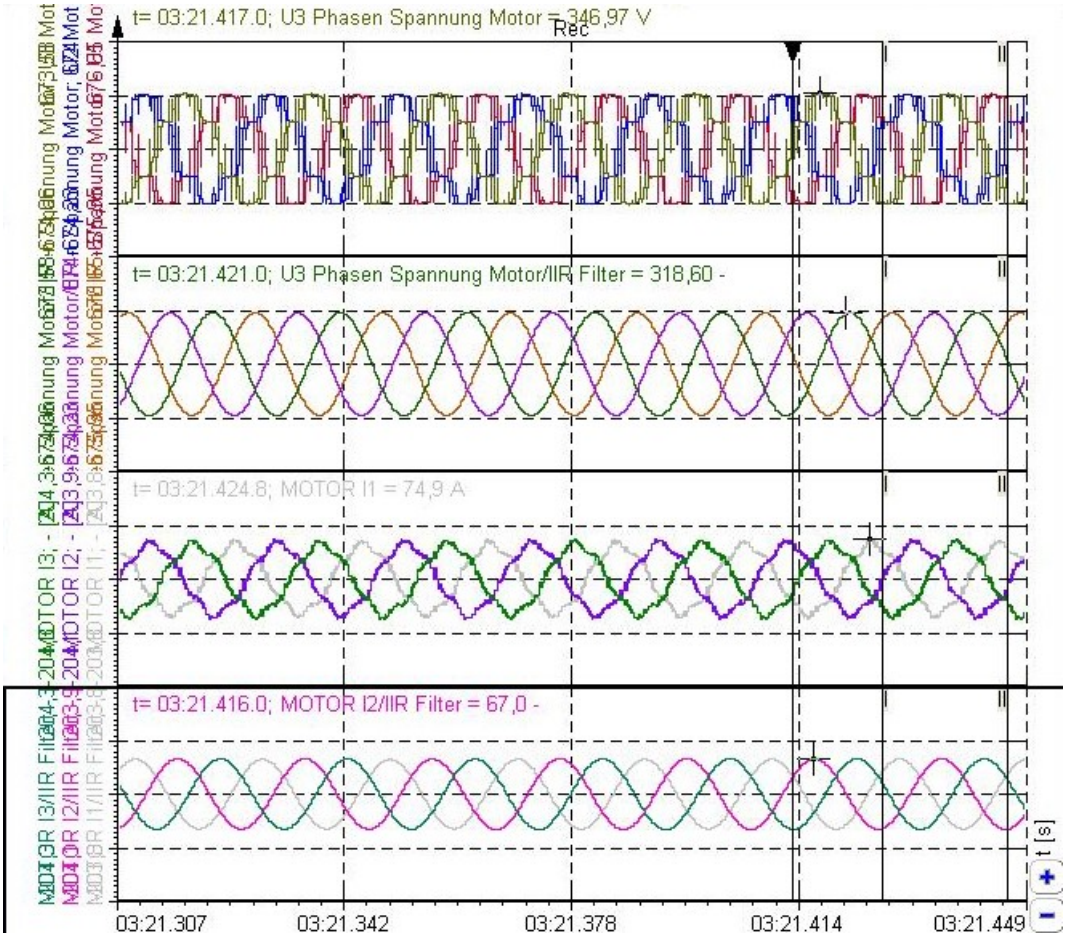

Figure 34 Filtered (bottom) and unfiltered (top) phase voltage and current

The filtered signal is used as a trigger point for the quadratic root mean square to receive a precise effective value.

The power factor cos φ is calculated by dividing the active power by the apparent power (see Equation (29)).

$$\cos\varphi = \frac{P}{S} \tag{30}$$

The mechanical power is calculated with Equation (2) but the analogue signal is given in rpm and needs to be transformed in revolutions per second.

3.3 Test Stand Control System

The prime mover is controlled by the inverter SIMOVERT FC as mentioned in Chapter 3.1.3. In the commissioning of the inverter the motor name plate is typed into the inverters set point parameters. The image below shows a guide from the instruction manual on the necessary parameters to control the engine (parameters like engine type, voltage, frequency, efficiency etc.). No adjustments had to be done to the programing of the SIMOVERT FC since the prime mover will be speed controlled.

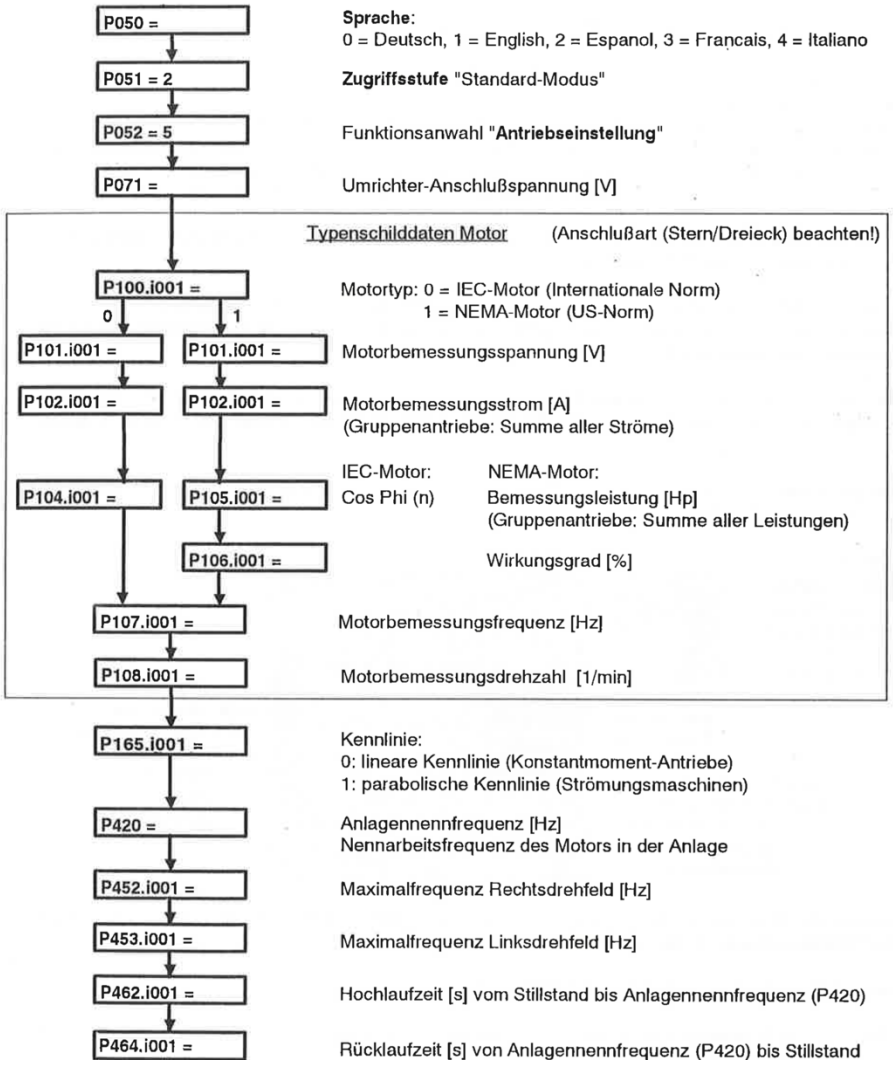

Figure 35 Motor name plate parameter entry

The pump simulator is controlled by the inverter SIMOVERT P. As for the SIMOVERT FC the crucial engine data from the motor name plate has to be saved to run the inverters control programs. A speed limit is programmed into the inverter to protect the equipment and the engine itself. The pump simulator will be torque controlled to recreate the pumping motion, the analogue input of the inverter is limited at 10 Volts to 200% of the torque set point. The analogue input is connected then to a function generator TG320. With the function generator the movement of the pump can be

determined by using a sinusoidal signal. The SPM and the amount of torque used for the upstroke can be adjusted by changing the Amplitude and the frequency.

Chapter 4 Experiments

4.1 Determination of engine capacity

The aim of the experiment was the complete measurement of an asynchronous machine (prime mover) to determine the equivalent circuit diagram (see Figure 36). With the measured data and the determined values of the equivalent circuit diagram, the current diagram of the asynchronous machine is created. The entire experiment is composed of 4 partial tests, namely the resistance measurement, the idling, the short-circuit and the load test.

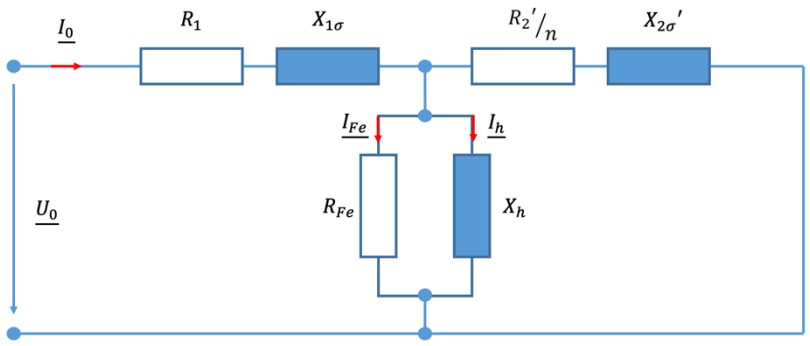

Figure 36Equivalent circuit diagram

4.1.1 Short circuit Test

For the short circuit experiment the prime mover was disconnected from the SIMOVERT FC VSD drive and connected to a variable transformer. The shaft must be jammed in place with tension straps for this experiment. Then it is important that the voltage is not directly and quickly upshifted to the nominal voltage, but in such small steps that the rated current of 35 amperes is not exceeded (see Figure 37).

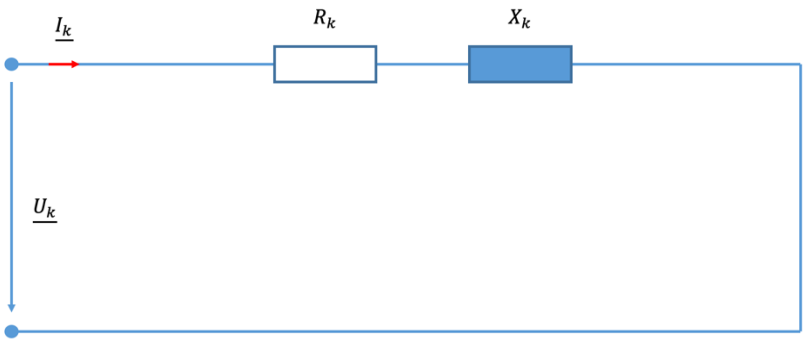

Figure 37 Short circuit Test

The measured result from the short circuit experiment can be seen in the table below.

Measured Properties	Results	Unit
$U_{k\ meas.}$	30,72	[V]
$I_{k\ meas.}$	33,63	[A]
$\varphi_{k\ meas.}$	59,79	[°]
$S_{k\ meas.}$	3,10	[kVA]
$P_{k\ meas.}$	1,56	[kW]
$Q_{k\ meas.}$	2,68	[kvar]
$\cos\varphi_{k\ meas.}$	0,50	[-]

Table 3 Results from short circuit experiment

The measured short circuit voltage U_k is the average voltage from the three phases combined. The same was done for the short circuit current I_k.

Since the nominal voltage was still far from being reached at 35 amps, the measurement data had to be converted to the rated voltage during evaluation by a constant factor k.

$$k = \frac{U_1}{U_{k\ meas.}} \tag{31}$$

The nominal current is calculated by multiplying the measured current $I_{k\ meas.}$ with the factor k. With the nominal voltage known and the nominal current estimated the leakage resistance can be calculated according to the formula below.

$$\underline{Z_k} = \frac{\underline{U_k}}{\underline{I_k}} \tag{32}$$

The complex leakage resistance also known as the short circuit impedance can be represented in Cartesian coordinates where R is the active resistance and X represents the reactive resistance(33).

$$\underline{Z_k} = R_k + jX_k \tag{33}$$

The stator resistor R_1 of the three windings is measured with a multi meter and the average value out of the three phases together is taken. The results are displayed in the table below

Stator windings	Result	Unit
$R_{stator\ phase\ 1}$	0,2788	[Ω]
$R_{stator\ phase\ 2}$	0,2796	[Ω]
$R_{stator\ phase\ 3}$	0,2786	[Ω]
R_1	0,2790	[Ω]

Table 4 Stator Resistance

The rotor resistance is calculated by subtracting the stator resistance from the real resistance from the short circuit impedance.

$$R_2' = R_k - R_1 \tag{34}$$

The complex part of the stator and rotor impedance is calculated by the formula below.

$$X_{1\sigma} = \frac{R_1}{R_k} * X_k \tag{35}$$

$$X_{2\sigma'} = \frac{R_2'}{R_k} * X_k \tag{36}$$

Calculating the formulas the stator impedance is 0,28 + 0,48j Ω and the rotor impedance is 0,18 + 0,31j Ω. Displayed in polar coordinates Z_1 is 0,55 ∠ 59,79° and Z_2' is 0,36 ∠ 59,79°.

4.1.2 Idling Test

Since in the short circuit experiment the ohmic resistance of the stator, the rotor and the rotor windings has been determined the copper losses can be calculated. The idling test also known as "no-load test" let's the engine run at its rated speed with no load on the shaft. The experiment has been done based on the Norm IEC 60034-2, where the experiment is performed in a no load scenario until the electrical power loss varies with no more than 3%. The measurement results from the experiment can be seen in the table below.

Measured Properties	Results	Unit
$U_{0\ meas.}$	273,73	[V]
$I_{0\ meas.}$	11,33	[A]
$\varphi_{0\ meas.}$	-74,29	[°]
$S_{0\ meas.}$	9,27	[kVA]
$P_{0\ meas.}$	2,51	[kW]
$Q_{0\ meas.}$	8,92	[kvar]
$\cos\varphi_{0\ meas.}$	0,27	[-]
$n_{0\ meas.}$	1494,00	[rpm]

Table 5 Measured results from Idling test

The phase angle of the voltage $U_{0\ meas.}$ is 0 and the current $I_{0\ meas.}$ is -74,29°. Therefore, the phase shift is 74,29° (see Equation(37))

$$\varphi_U - \varphi_I = \varphi_{UI} \tag{37}$$

Dividing the voltage $U_{0\ meas.}$by the current $I_{0\ meas.}$the impedance Z_0 is calculated (see Equation below).

$$Z_0 = \frac{U_{0\ meas.}}{I_{0\ meas.}} \tag{38}$$

The impedance Z_0 includes the stator impedance Z_1 and the impedance from the iron losses Z_h plus the main inductivity.

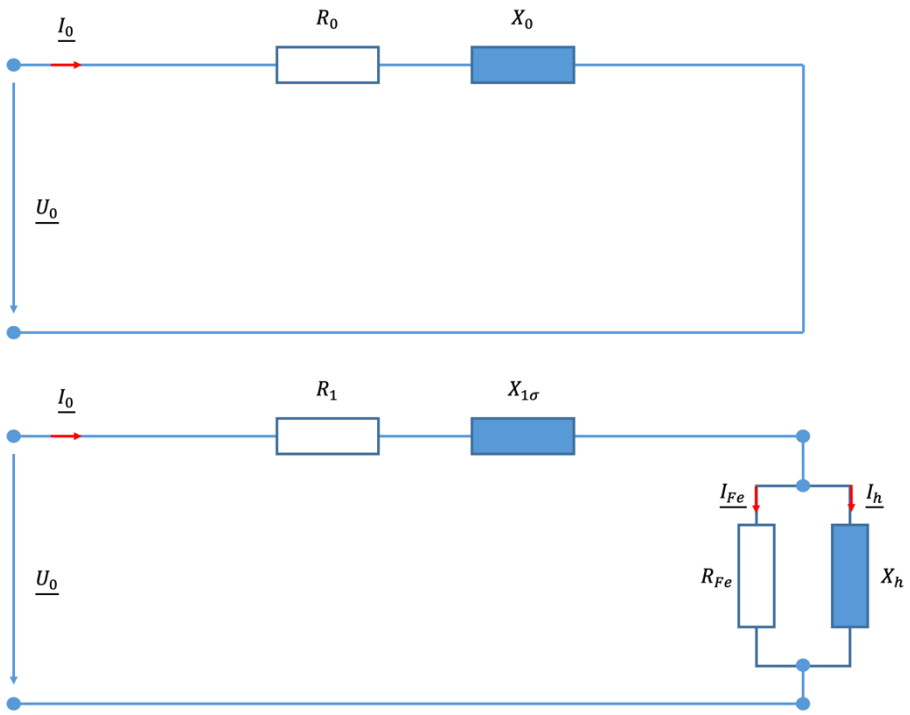

Figure 38 Idling test

But to calculate the iron core resistance R_{Fe} and the magnetizing inductance X_h the admittance of $\underline{Z_h}$ is calculated where $\frac{1}{G_h}$ is the iron resistance and $\frac{1}{B_h}$ is the magnetizing inductance (see Equation (39)&(40)).

$$\underline{Z_h} = \underline{Z_0} - \underline{Z_1} \tag{39}$$

$$\underline{Y_h} = \frac{1}{\underline{Z_h}} = \frac{1}{G_h} + \frac{1}{B_h} \tag{40}$$

The calculated results from the experiment can be seen in the table below.

Calculated Properties	Results	Unit
$\underline{Z_0}$	$23{,}81 \angle 74{,}31°$	[Ω]
$\underline{Z_h}$	$23{,}81 \angle 74{,}65°$	[Ω]
$\underline{Y_h}$	$0{,}04 \angle 74{,}65°$	[Ω]
R_{Fe}	87,91	[Ω]
X_h	24,13	[Ω]

Table 6 Results from idling experiment

The power losses from the copper winding P_{cu1} and the iron core P_{fe} is calculated with the formulas below where the copper winding losses are 0,11 kW and the iron core losses are 2,40 kW.

$$P_{Cu1} = 3 * R_1 * I_{0\,meas.}^2 \quad (41)$$

$$P_{Fe} = P_{0\,meas.} - P_{Cu1} \quad (42)$$

4.2 Current locus of the prime mover

The Ossanna circle diagram is the representation of the current locus of a three-phase asynchronous motor in the complex plane. It allows a relatively simple representation of power, torque and loss of the prime mover in generator and motor operation depending on the slip.

Given the phase voltage lies on the y- axis, the x-axis represents the imaginary current and the y axis the real current. At least three coordinates are necessary to create the current locus. Therefore, a third test has been performed to measure the current and the voltage of the prime mover at 100% of its load capacity. The Ossanna-circle is created by inserting the idling current (coordinates is represented as P_0), the short circuit current (coordinates is represented as P_1) and the current from the constant load experiment (coordinates represented as P_N) into the graph below. The three currents used to create the locus are shown in the table below.

Coordinate	X [imaginary Amps]	Y [real Amps]
P_0	-11,7	3,11
P_N	-36,92	39,22
P_1	-218,47	127,22

Table 7 Coordinates for Ossanna-circle

The half way point between $P_1$and P_0 is perpendicular to the centre of the locus, the same applies also toP_N and P_0, hence where the two perpendiculars cross marks the centre point of the Ossanna-circle. Once the centre point of the current locus is determined the circle can be drawn which passes through the coordinates P_0, P_N and P_1.

The line between P_0 and P_1 is known as the power line. To draw the torque line the midpoint line has to be drawn which connects the centre point to P_0. Perpendicular from the midpoint line to P_1 the relationship applies $\overline{P_1B} = \frac{\overline{P_1A}}{2}$ (the coordinate A represent the perpendicular on the x axis to P_1 and the coordinate B represents the crossing point on the torque line from perpendicular midpoint line to P_1). With position B the torque line can be drawn as it can be seen in the figure below.

Once the torque line is drawn the break-over point of the induction motor can be drawn by drawing a perpendicular line from the torque line through the midpoint.

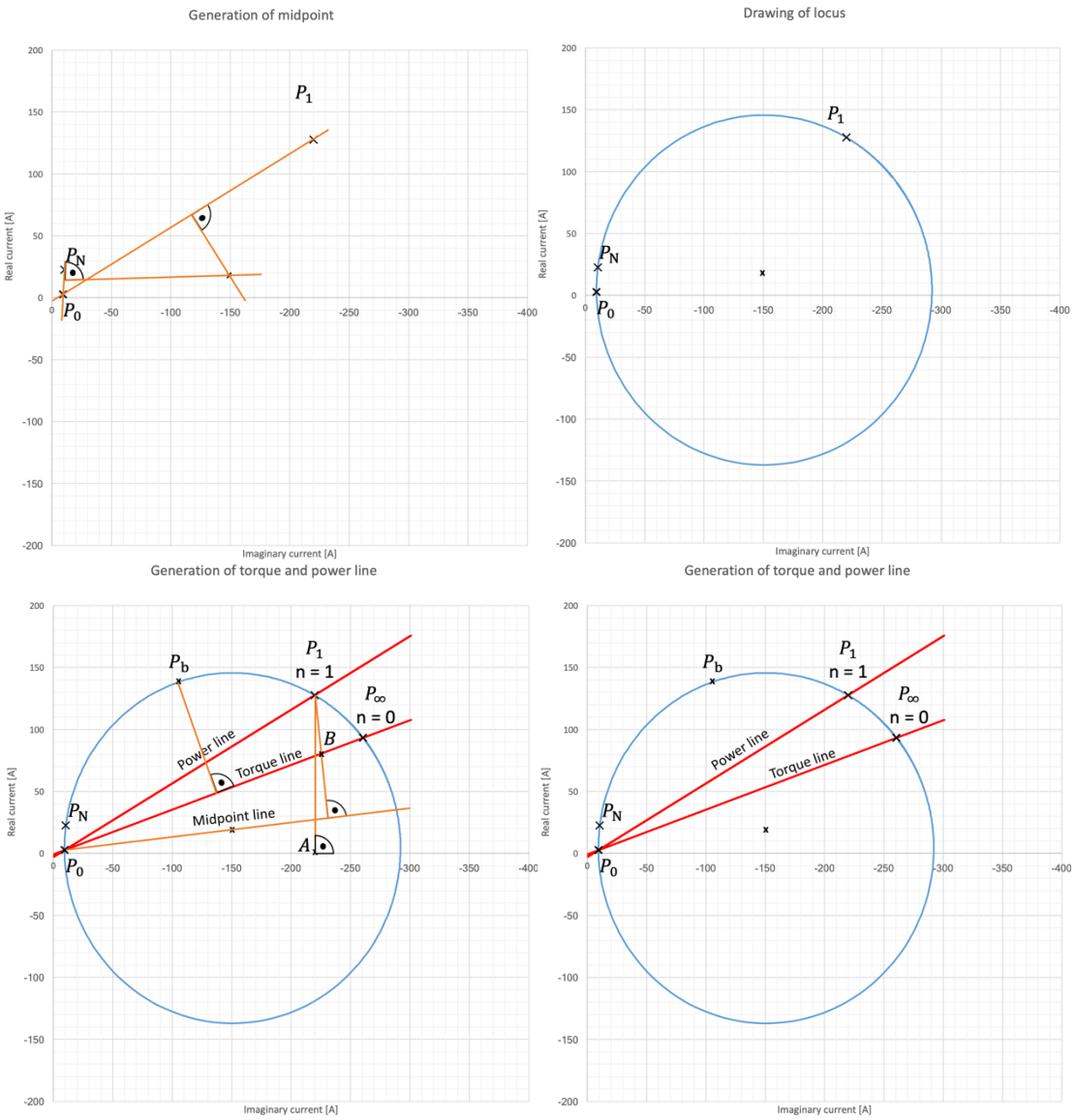

Graph 7 Ossanna locus creation

From the power line not only the mechanical and electrical power of the engine can be seen on the current locus diagram but also its losses are represented. The starting torque and break-over point can be measured from the torque line. Based on the Ossanna locus the torque vs speed, efficiency vs speed, current vs speed and the power vs speed diagram (Graph 8) can be drawn by applying the current scale m_1 in the Unit A/cm, the power scale m_p in W/cm and the torque scale m_M in Nm/cm as it can be seen in the equations below.

$$m_p = 3 * U_1 * m_1 \tag{43}$$

$$m_M = 9{,}55 * \frac{m_p}{n_1} \tag{44}$$

The graphs in the Figure below do now only show the engines performance but also proves that the prime mover is a IE3 engine.

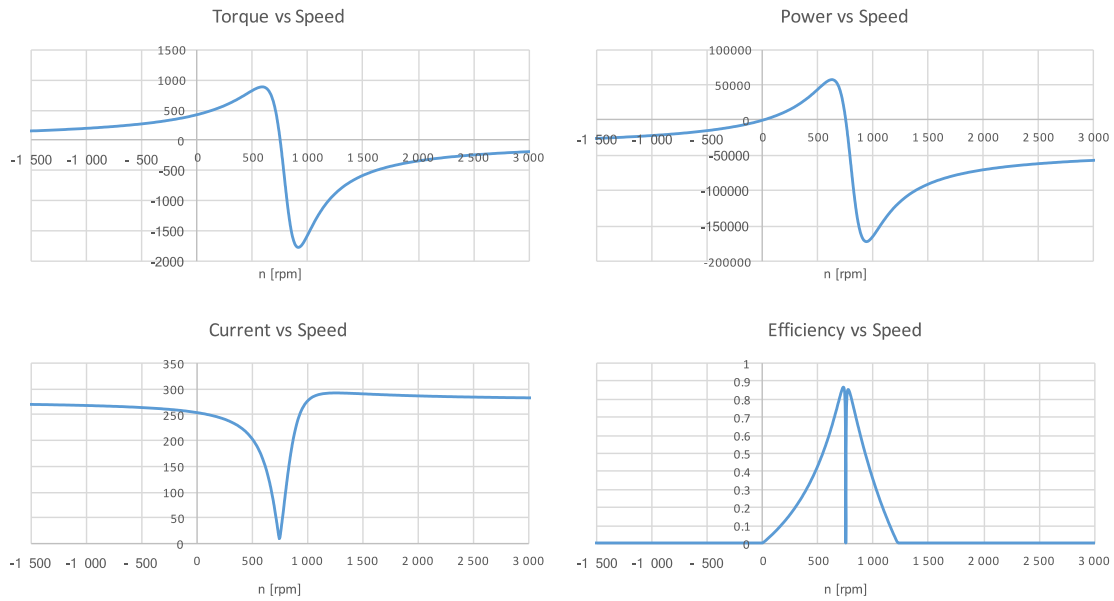

Graph 8 Results from Ossanna locus

4.3 Pumping Simulation

As mentioned in Chapter 3.3 the pump simulator will be torque controlled by a function generator with a sinusoidal signal. The function of the signal can be seen in the Equations below. The used parameters for the pumping simulation can be observed in Figure 39.

$$y(t) = A * \sin(\omega * t) \tag{45}$$

$$\omega = 2 * \pi * f \tag{46}$$

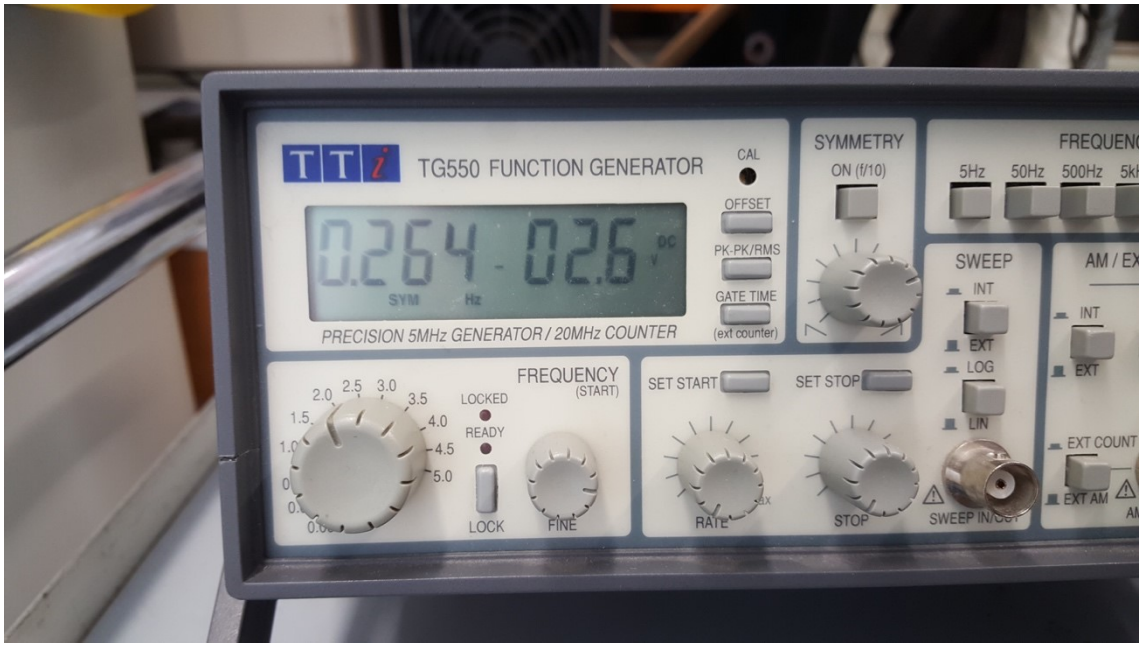

Figure 39 Function generator input parameters

The Amplitude of the signal is 2,6 Volts and has a frequency of 0,264 Hz, this results in the pump simulator generating 16 SPM with a maximum torque of 169 Nm.

The generated function is displayed in an oscilloscope as it can be seen in the figure below. It can be seen that the sinusoidal signal is not fully symmetrical. This effect is to be expected in the field as well.

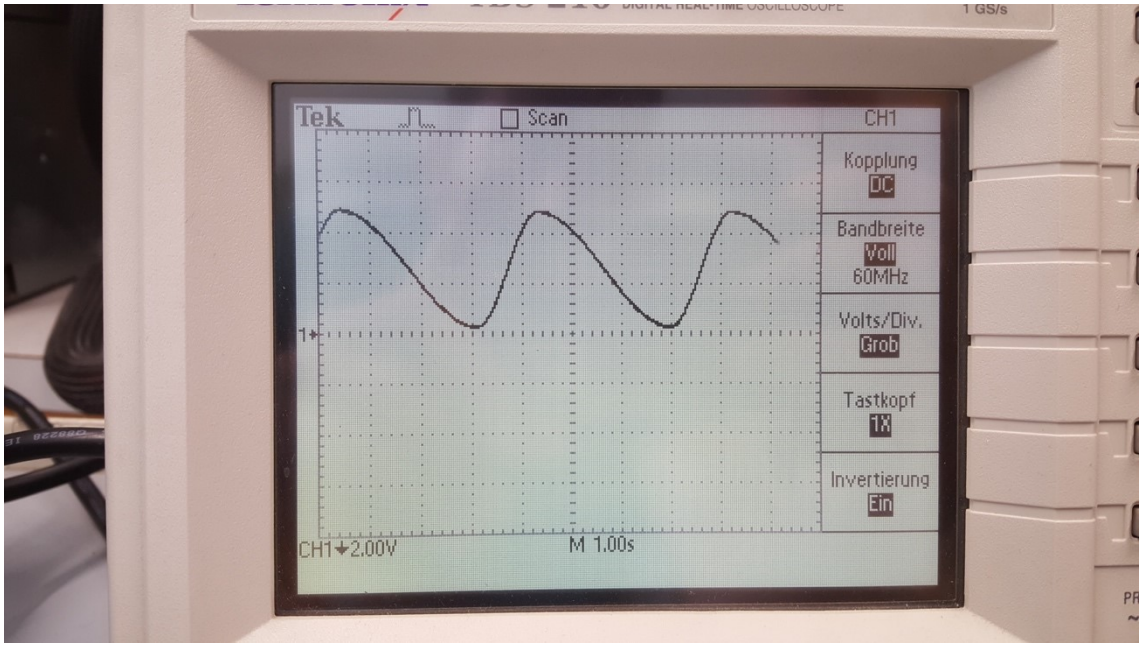

Figure 40 pump simulator input signal

In the graph below the torque is represented by the data analysis software Dewesoft in red. One can see how the speed of the prime mover is reduced due to the increase of the torque by the pump simulator on the prime mover.

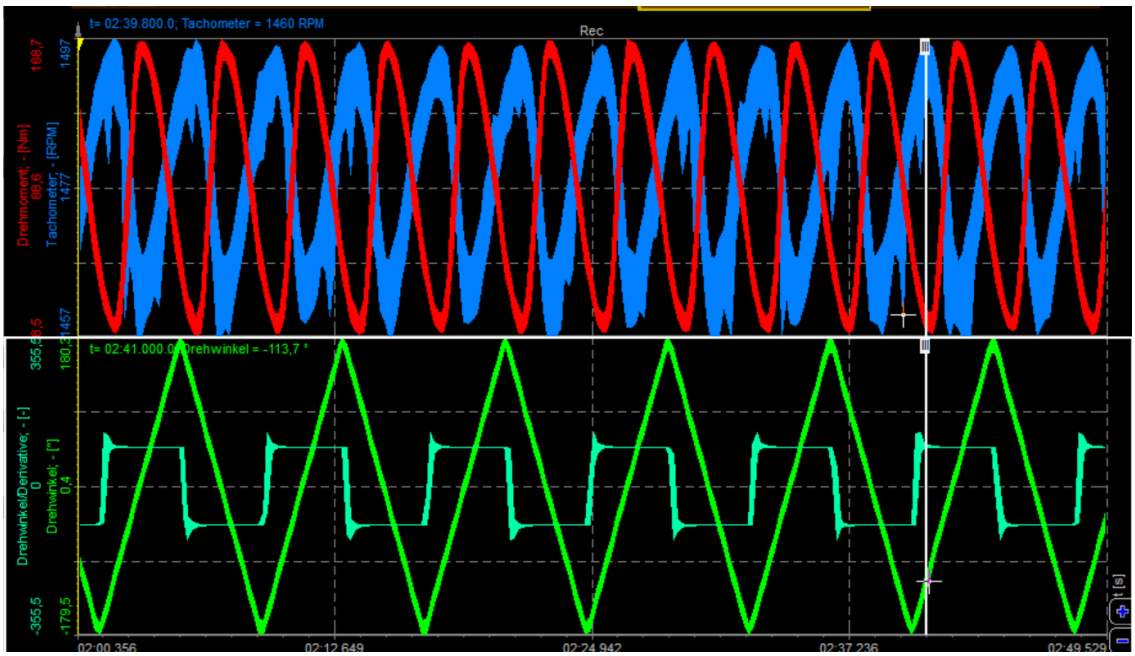

Figure 41 pump simulation representation of rotational angle, torque and speed

The turquoise line in Figure 41 represents every stroke the pump simulator simulates; the green line shows the position of the shaft of the test stand. As discussed in Chapter 3.2.2 the shaft positioning sensor simulates the position of the counterweights. Two torque peaks should have been observed in on stroke. One peak that represents the lifting of the sucker rod strings with the produced fluids and a second lower torque peak that represents the counterweights. The reason that the two peaks are equally high is that the settings of the function generator gives the torque of the counter weights as high as the torque of the lifted fluids. Figure 42 shows the position of the shaft in terms of the up and down stroke of the sucker rod pump.

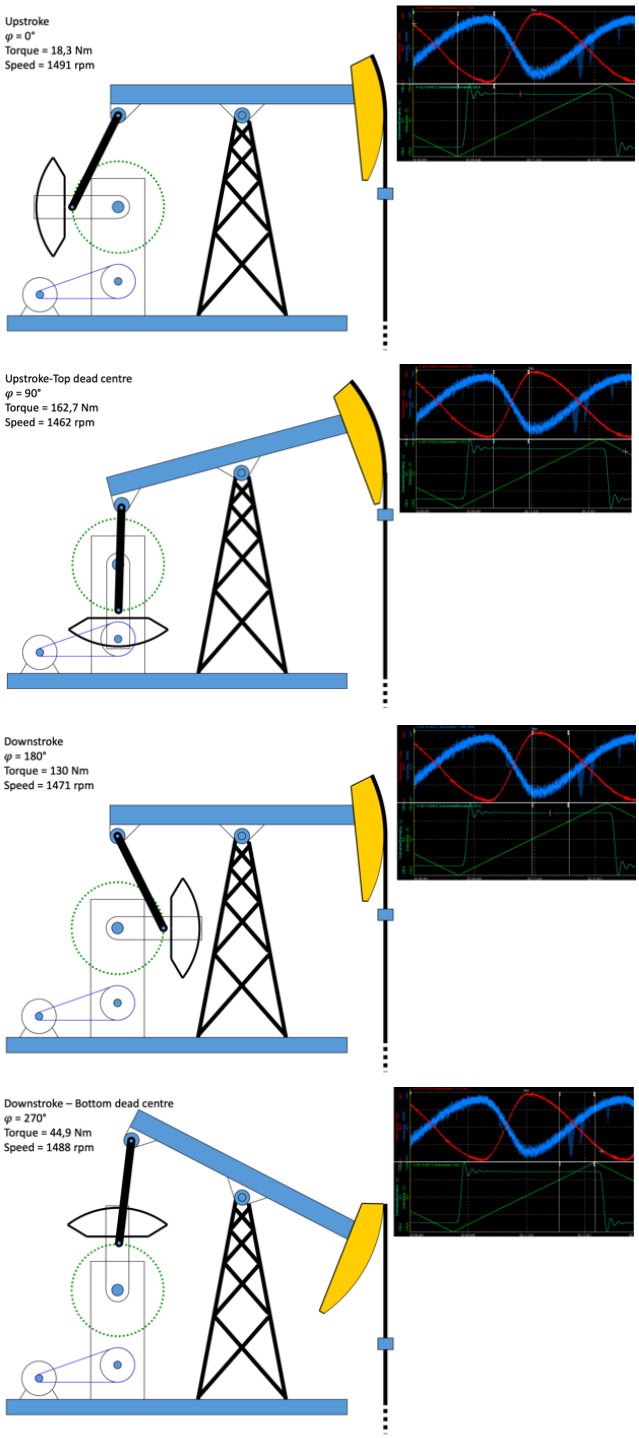

Figure 42 Up and down stroke representation in Dewesoft

In the figure below it can be observed how the mechanical power output (purple) of the system changes simultaneously with the measured torque (light red) and the prime movers power output (light green) and reciprocally to the systems mechanical power output the pump simulators output (dark red) and the reduction in rpm (blue).

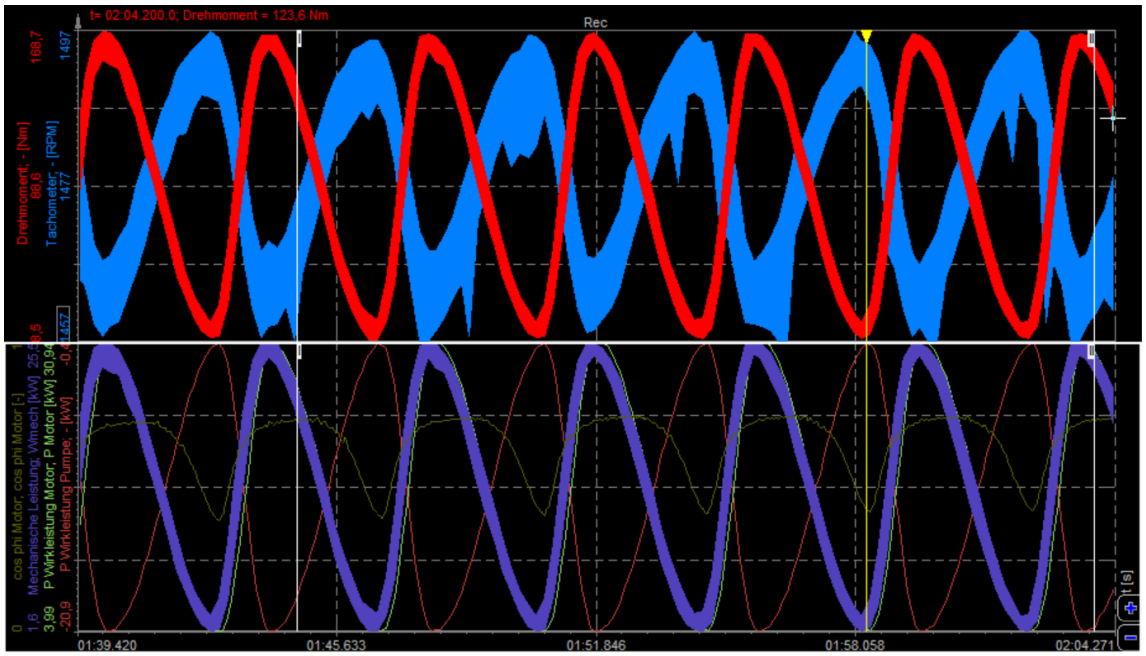

Figure 43 Torque vs Power pumping experiment

The peak mechanical power output of the system is 24,6 kW, the peak output of the motor is 30,8 kW and of the pump it is 20,8 kW. To see if the performance of the simulator is accurate and comparable to real life data the performance of an actual sucker rod pump from the Oil Production Company OMV in Bockfließ is compared to the pump simulator results.

Figure 44 Sucker rod pump in Bocklfieß

The sucker rod pump in Bockfließ is also an IE2 motor with similar features. The image below shows the systems performance and the polished rod position with the force of the plunger.

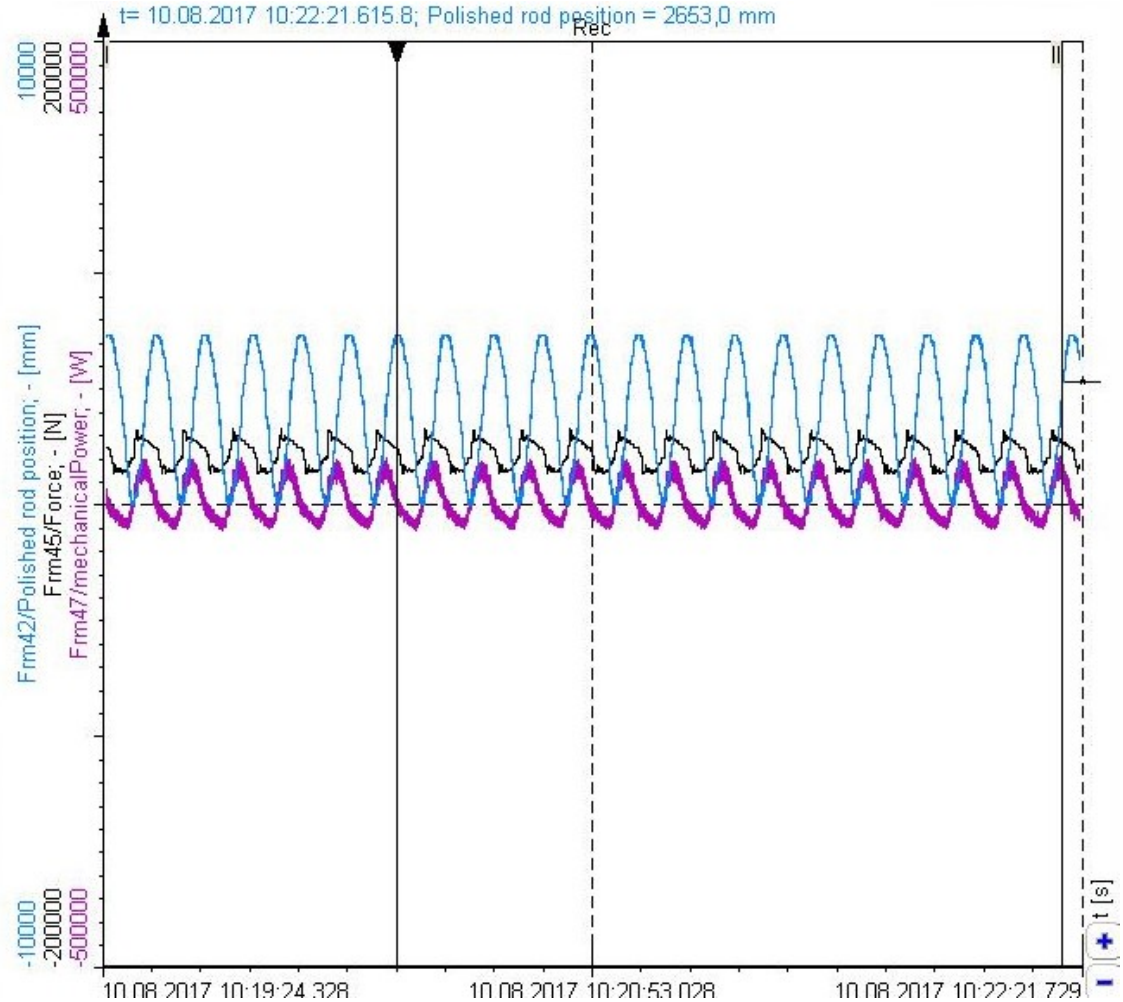

Figure 45 Results from the sucker rod pump in Bockfließ

The results from Bockfließ reflect the pump simulators performance on not only the display of the torque simulator but also the positioning sensor that indicates at what point the stroke commences.

Chapter 5 Conclusion

The aim of the thesis is to build a test stand where a prime movers performance during a simulated pumping operation can be observed. The goal has been achieved by connecting successfully the prime mover over the shaft to the second engine that simulates the pump. The difficulty of connecting the two engines was represented not only by fitting the two shafts to a custom made clutch but also by elevating the smaller pump simulator to the correct height in order to connect the two engines over the shaft. Additional challenges have been identified when the engines had to be mounted safely to the machine table. Originally it was planned to build the test stand on an elevated surface to improve the ergonomic working condition during maintenance work, but in consideration of the prime mover's weight (a total of 360 k) it was considerably easier to build the test stand on the floor.

In order to observe both engines performances the next goal has been to construct a solid measurement system that not only measures the incoming and outgoing voltages and currents of the prime mover but is also capable of measuring the torque, speed and rotational angle of the shaft. The measurement system also has to be able to differentiate between line to line voltage, phase voltage and effective voltage. The same also applies to the line to line current, phase current and effective current. This has been accomplished by successfully linking the test stand measurement instruments to the data acquisition card of the PC and calibrating the incoming signals to the correct unit.

The most time consuming process was soldering the measurement control system, shaft positioning sensor and differential amplifier. Defilements on the circuit board are normally hard to spot and lead to disturbances on the outgoing signal and to short circuits. Circuit board contaminations were not the only error source in the measurement units. The outgoing signal had to be stabilized by experimenting with different resistors, capacitors and microchips. Since there were several measurement processes simultaneously, the risk of not only electromagnetic disturbances but also of the measurement units influencing one and another was potentially high. Therefore, every circuit board and measurement cable had to be isolated and decoupled from outside disturbances. Once the errors from the measurement system have been mitigated a reference signal is used to verify the measurements outcome. This process had to be carried out for every signal channel. The measurement units had to be labelled carefully to avoid wrong measurements or even connecting one of the units to the wrong power supply as this could damage the costly precision resistors or the microchips. In order to protect these components from high voltage charges, opto-isolators have been installed.

Once the test stand was built with the measurement system, it had to be dismantled again for the idling and short circuit test in order to understand the engines characteristics. This was necessary as the prime mover was in operation for 30 years until 2001. Spec sheets to the engine were therefore no longer available for

consultation. The idling and short circuit test confirmed that the engine operates in the power range of IE3 motors.

The final target of the thesis is a control system to simulate the sucker rod pump movement by the torque controlled pump simulator and the speed controlled prime mover. The available VSD drive of the prime mover was not applicable to the engines specs, therefore adjustments had to be made to meet the engines capacity.

Via familiarising with the VSD programming manuals and using a function generator as an input signal for the torque control pump simulator interface, an approximate up and down stroke has been simulated on the test stand.

The test stand allows to simulate pumping operations and observing the performance of the prime mover in a save and controlled environment. With the advanced measurement system mathematical models can be developed to further understand the overall behaviour and performance of the system.

The possibility of simulating certain scenarios and quantifying them based on a model, can lead to substantial improvements in powering a sucker rod pump efficiently. One of the improvements would involve reducing power peaks caused by the resonance effects of the rods, powering the pump in a frequency elastic mode. This would not only reduce maintenances for the work-over team but also reduce energy costs generated by the power grid.

Further possible improvements to the test bench could involve adding a B20 X20 generation B & R controller to the existing pump simulation test bench. Once implemented, this control could take on a variety of tasks, including the measurement and processing of sensor signals, the speed control of the motor and the storage of measurement data in a database.

Appendix

1. Device specifications NI 6220

M Series Data Acquisition: 16-Bit, 250 kS/s, 16 AI, 24 DIO

The following specifications are typical at 25 °C, unless otherwise noted. For more information about the NI 6220, refer to the *M Series User Manual* available at *ni.com/manuals*.

Analog Input

Number of channels	8 differential or 16 single ended
ADC resolution	16 bits
DNL	No missing codes guaranteed
INL	Refer to the *AI Absolute Accuracy* section
Sample rate	
Single channel maximum	250 kS/s
Multichannel maximum (aggregate)	250 kS/s
Minimum	No minimum
Timing accuracy	50 ppm of sample rate
Timing resolution	50 ns
Input coupling	DC
Input range	±0.2 V, ±1 V, ±5 V, ±10 V
Maximum working voltage for analog inputs (signal + common mode)	±11 V of AI GND
CMRR (DC to 60 Hz)	92 dB
Input impedance	
Device on	
AI+ to AI GND	>10 GΩ in parallel with 100 pF
AI- to AI GND	>10 GΩ in parallel with 100 pF

Device off	
AI+ to AI GND	820 Ω
AI- to AI GND	820 Ω
Input bias current	±100 pA
Crosstalk (at 100 kHz)	
Adjacent channels	-75 dB
Non-adjacent channels	-90 dB
Small signal bandwidth (-3 dB)	700 kHz
Input FIFO size	4,095 samples
Scan list memory	4,095 entries
Data transfers	DMA (scatter-gather), interrupts, programmed I/O
Overvoltage protection for all analog input and sense channels	
Device on	±25 V for up to two AI pins
Device off	±15 V for up to two AI pins
Input current during overvoltage condition	±20 mA maximum/AI pin

Settling Time for Multichannel Measurements

Accuracy, full-scale step, all ranges	
±90 ppm of step (±6 LSB)	4 µs convert interval
±30 ppm of step (±2 LSB)	5 µs convert interval
±15 ppm of step (±1 LSB)	7 µs convert interval

Recommended Operating Conditions

Level	Minimum	Maximum
Input high voltage (V_{IH})	2.2 V	5.25 V
Input low voltage (V_{IL})	0 V	0.8 V
Output high current (I_{OH}) P0.<0..7>	—	-24 mA
Output high current (I_{OH}) PFI <0..15>/P1/P2	—	-16 mA
Output low current (I_{OL}) P0.<0..7>	—	24 mA
Output low current (I_{OL}) PFI <0..15>/P1/P2	—	16 mA

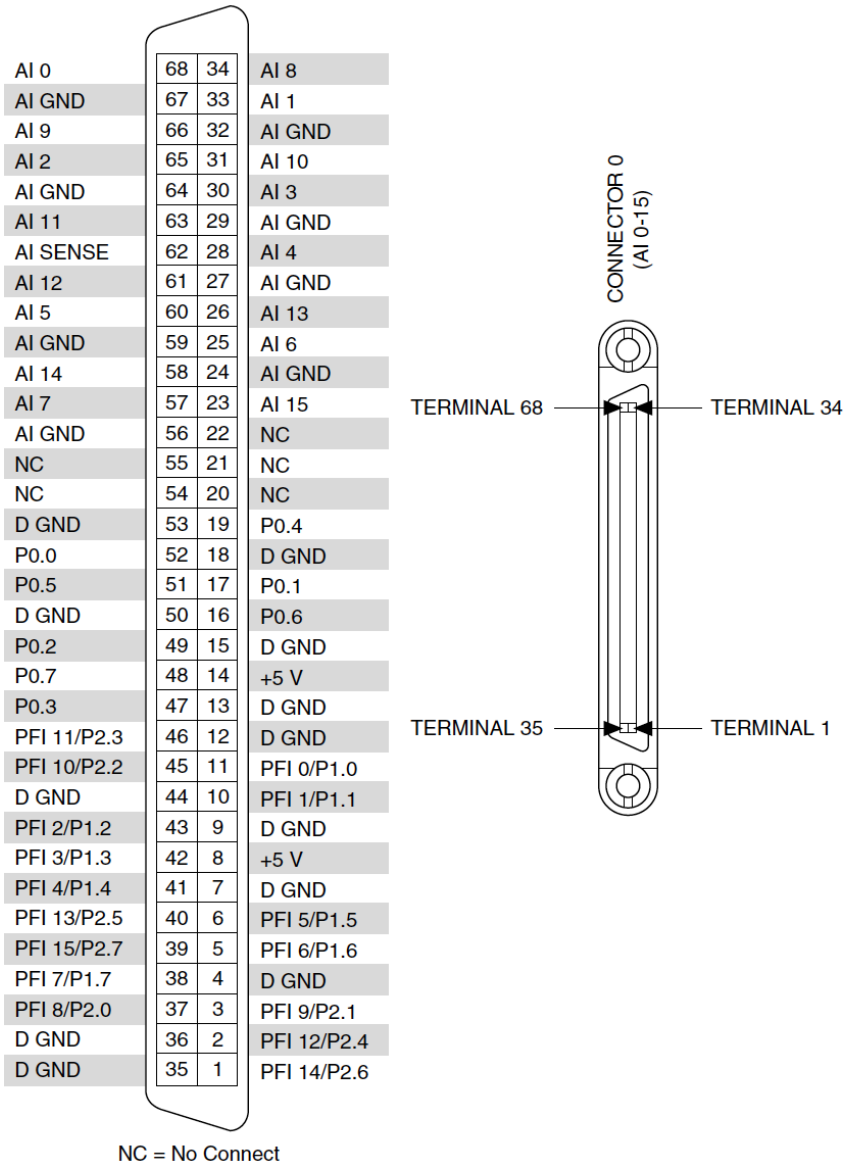
AI 0 68 34 AI 8
AI GND 67 33 AI 1
AI 9 66 32 AI GND
AI 2 65 31 AI 10
AI GND 64 30 AI 3
AI 11 63 29 AI GND
AI SENSE 62 28 AI 4
AI 12 61 27 AI GND
AI 5 60 26 AI 13
AI GND 59 25 AI 6
AI 14 58 24 AI GND
AI 7 57 23 AI 15
AI GND 56 22 NC
NC 55 21 NC
NC 54 20 NC
D GND 53 19 P0.4
P0.0 52 18 D GND
P0.5 51 17 P0.1
D GND 50 16 P0.6
P0.2 49 15 D GND
P0.7 48 14 +5 V
P0.3 47 13 D GND
PFI 11/P2.3 46 12 D GND
PFI 10/P2.2 45 11 PFI 0/P1.0
D GND 44 10 PFI 1/P1.1
PFI 2/P1.2 43 9 D GND
PFI 3/P1.3 42 8 +5 V
PFI 4/P1.4 41 7 D GND
PFI 13/P2.5 40 6 PFI 5/P1.5
PFI 15/P2.7 39 5 PFI 6/P1.6
PFI 7/P1.7 38 4 D GND
PFI 8/P2.0 37 3 PFI 9/P2.1
D GND 36 2 PFI 12/P2.4
D GND 35 1 PFI 14/P2.6
NC = No Connect
CONNECTOR 0
(AI 0-15)
TERMINAL 68
TERMINAL 34
TERMINAL 35
TERMINAL 1

1.1. Spec sheet of the current transducer

Current Transducer LT 200-S

I_{PN} = 200 A

For the electronic measurement of currents : DC, AC, pulsed..., with a galvanic isolation between the primary circuit (high power) and the secondary circuit (electronic circuit).

16226

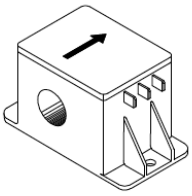

Electrical data

I_{PN}	Primary nominal current rms		200		A
I_{PM}	Primary current, measuring range		0 .. ± 300		A
R_M	Measuring resistance		$R_{M\,min}$	$R_{M\,max}$	
	with ± 12 V	@ ± 200 A_{max}	0	65	Ω
		@ ± 300 A_{max}	0	30	Ω
	with ± 18 V	@ ± 200 A_{max}	50	120	Ω
		@ ± 300 A_{max}	50	65	Ω
I_{SN}	Secondary nominal current rms		100		mA
K_N	Conversion ratio		1 : 2000		
V_C	Supply voltage (± 5 %)		± 12 .. 18		V
I_C	Current consumption		28 (@±18V)+ I_S		mA

Accuracy - Dynamic performance data

X	Accuracy @ I_{PN}, T_A = 25°C		± 0.5		%
ε_L	Linearity error		< 0.1		%
			Typ	Max	
I_O	Offset current @ I_P = 0, T_A = 25°C			± 0.3	mA
I_{OM}	Magnetic offset current @ I_P = 0 and specified R_M, after an overload of 3 x I_{PN}			± 0.2	mA
I_{OT}	Temperature variation of I_O	0°C .. + 70°C	± 0.3	± 0.5	mA
t_r	Response time [1] to 90 % of I_{PN} step		< 1		µs
di/dt	di/dt accurately followed		> 50		A/µs
BW	Frequency bandwidth (-1dB)		DC .. 150		kHz

General data

T_A	Ambient operating temperature		0 .. + 70	°C
T_S	Ambient storage temperature		- 25 .. + 85	°C
R_S	Secondary coil resistance @ T_A = 70°C		35	Ω
m	Mass		200	g
	Standards		EN 50178: 1997	

Features

- Closed loop (compensated) current transducer using the Hall effect
- Transducer with isolated plastic case recognized according to UL 94-V0.

Advantages

- Excellent accuracy
- Very good linearity
- Low temperature drift
- Optimized response time
- Wide frequency bandwidth
- No insertion losses
- High immunity to external interference
- Current overload capability.

Applications

- AC variable speed drives and servo motor drives
- Static converters for DC motor drives
- Battery supplied applications
- Uninterruptible Power Supplies (UPS)
- Switched Mode Power Supplies (SMPS)
- Power supplies for welding applications.

Application domain

- Industrial.

1.2. Spec sheet of the voltage transducer

LEM

Voltage Transducer LV 100

I_{PN} = 10 mA
V_{PN} = 100 .. 2500 V

For the electronic measurement of voltage: DC, AC, pulsed..., with galvanic isolation between the primary circuit and the secondary circuit.

Electrical data

I_{PN}	Primary nominal current rms		10		mA
I_{PM}	Primary current, measuring range		0 ± 20		mA
R_M	Measuring resistance		$R_{M\,min}$	$R_{M\,max}$	
	with ± 15 V	@ ± 10 mA $_{max}$	0	150	Ω
		@ ± 20 mA $_{max}$	0	50	Ω
I_{SN}	Secondary nominal current rms		50		mA
K_N	Conversion ratio		10000 : 2000		
V_C	Supply voltage (± 5 %)		± 15		V
I_C	Current consumption		31 + I_S		mA

Accuracy - Dynamic performance data

X_G	Overall accuracy @ I_{PN}, T_A = 25°C		± 0.7		%
ε_L	Linearity error		< 0.1		%
			Typ	Max	
I_O	Offset current @ I_P = 0, T_A = 25°C			± 0.2	mA
I_{OT}	Temperature variation of I_O	0°C .. + 70°C	± 0.2	± 0.3	mA
t_r	Response time [1] to 90 % of I_{PN} step		20 .. 100		µs

General data

T_A	Ambient operating temperature		0 .. 70	°C
T_S	Ambient storage temperature		- 25 .. + 85	°C
R_P	Primary coil resistance @ T_A = 70°C		1900	Ω
R_S	Secondary coil resistance @ T_A = 70°C		60	Ω
m	Mass		460	g
	Standards		EN 50178: 1997	

Note: [1] R_1 = 100 kΩ (L/R constant, produced by the resistance and inductance of the primary circuit).

Features

- Closed loop (compensated) voltage transducer using the Hall effect
- Isolated plastic case recognized according to UL 94-V0.

Principle of use

- For voltage measurements, a current proportional to the measured voltage must be passed through an external resistor R_1 which is selected by the user and installed in series with the primary circuit of the transducer.

Advantages

- Excellent accuracy
- Very good linearity
- Low temperature drift
- Optimized response time
- Wide frequency bandwidth
- High immunity to external interference
- Low disturbance in common mode.

Applications

- AC variable speed drives and servo motor drives
- Static converters for DC motor drives
- Battery supplied applications
- Uninterruptible Power Supplies (UPS)
- Power supplies for welding applications.

Application Domain

- Industrial.

1.3. Functional- / logic diagram and pinning information

1.3.1. HEF40106B

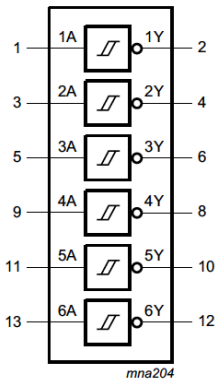

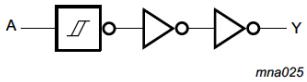

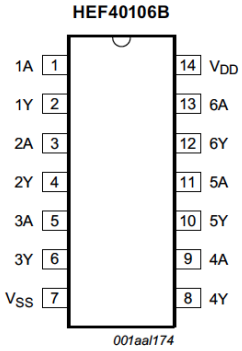

1.3.2. HEF4093B

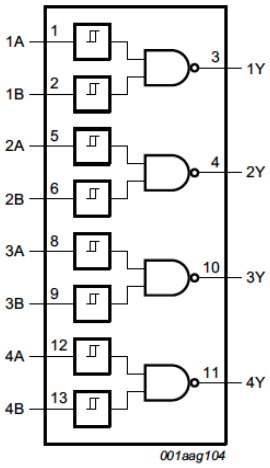

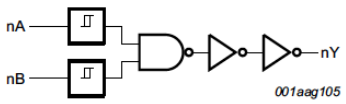

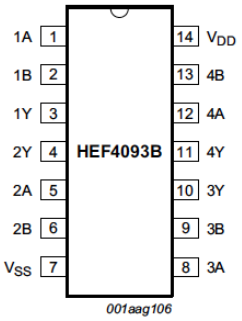

1.3.3. HEF4070B

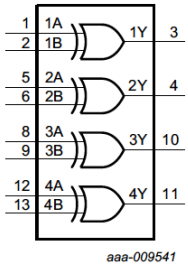

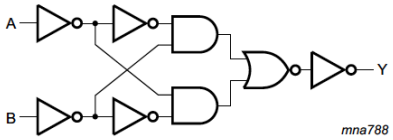

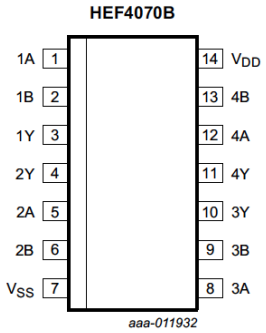

1.1.1. HEF4017B

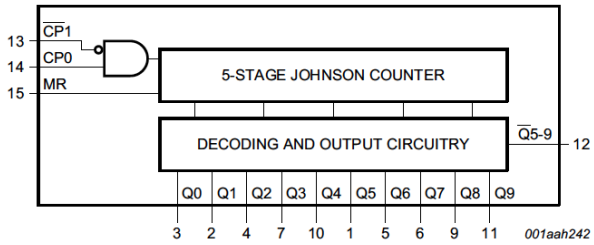

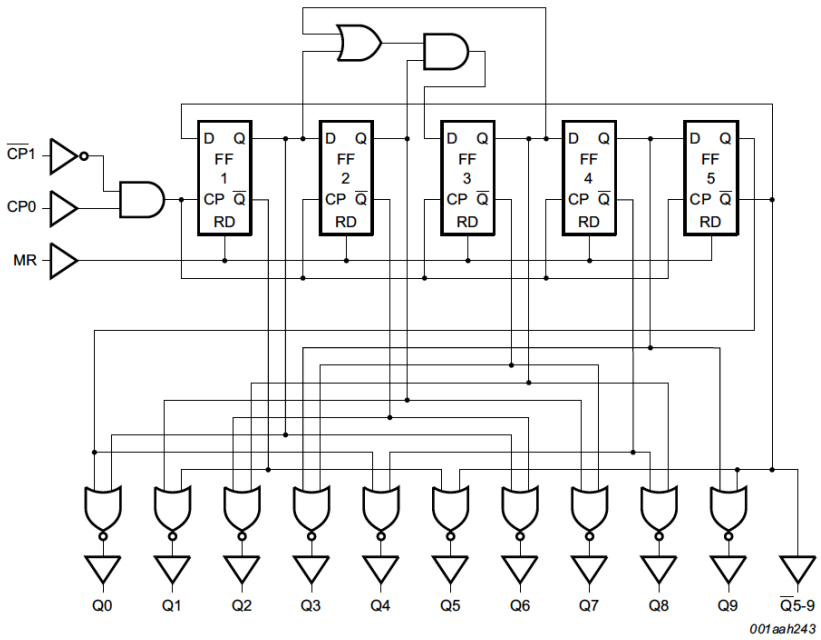

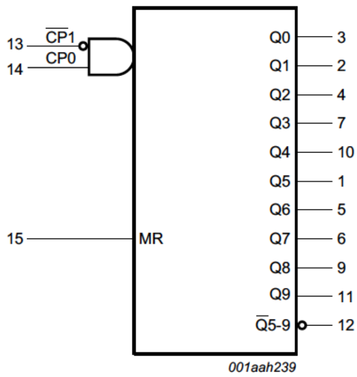

2. Measurement interface arrangement

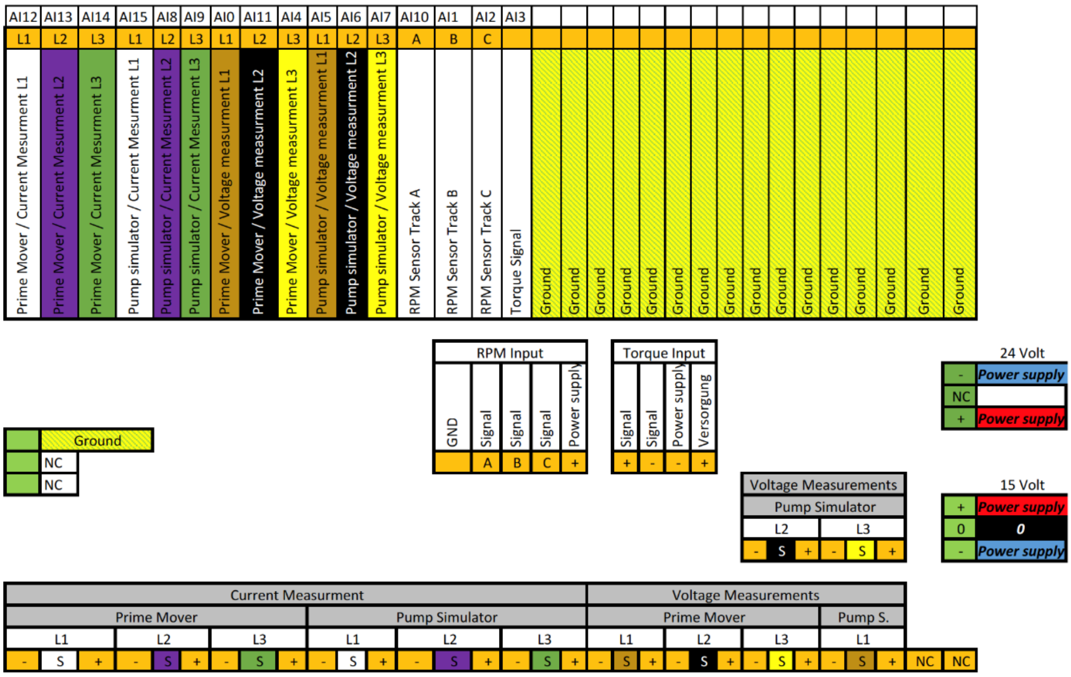

3. Signal calibration

3.1. Voltage transducer resistor selection

Measurements have been done with the Ohmmeter Fluke 189 with a reference error of:

DC voltage 0,025%

AC Voltage 0,4%

Measured Signal	**L1**	**L2**	**L3**
R+	50,150		
R-	49,940		
Ri	1,633		
R+		49,700	
R-		50,100	
Ri		1,634	
R+			50,300
R-			50,240
Ri			1,632
Sum	101,723	101,434	102,172
Pump simulator			
R+	49,746		
R-	50,210		
Ri	1,609		
R+		49,740	
R-		49,880	
Ri		1,620	
R+			50,140
R-			49,830
Ri			1,613
Sum	101,565	101,240	101,583

Necessary Sensing Resistor with less than 1% Error

Prime Mover				
Line Current	**L1**	**L2**	**L3**	
R_m	6200	7500	4700	kΩ
Pump simulator				
Line Current	**L1**	**L2**	**L3**	
R_m	6200	8200	6200	kΩ

3.2. Differential amplifier performance test

Measurements have been done with the Ohmmeter Fluke 189 with a reference error of:

DC voltage 0,025%

AC Voltage 0,4%

Amplifier	Input Volate [V]	Output Volate [V]	Amplification [-]
OPV-A1	5,2415	2,6270	0,50
OPV-A2	5,2917	2,6441	0,50
OPV-A3	5,2887	2,6466	0,50
OPV-A4	5,2863	2,6526	0,50
OPV-A5	5,2454	2,6286	0,50
OPV-A6	5,2868	2,6207	0,50
OPV-A7	5,2845	2,6537	0,50
OPV-A8	5,2855	2,6351	0,50
OPV-B1	5,287	2,6457	0,50
OPV-B2	5,2428	2,6234	0,50
OPV-B3	5,2858	2,6378	0,50
OPV-B4	5,2433	2,6181	0,50
OPV-B5	5,2855	2,6369	0,50
OPV-B6	5,2437	2,6215	0,50
OPV-B7	5,2860	2,6369	0,50
OPV-B8	5,2452	2,6262	0,50

3.3. Torque Sensor Calibration

Torque [Nm]	Measured [Nm]	Dewesoft [V]	Offset	Error	Skalierfaktor
0	-0,67	-0,0148	0,67		
10,00	9,8	0,248	0,20	2,03%	1,09
19,61	18,8	0,472	0,81	4,15%	1,08
29,32	28,1	0,706	1,22	4,17%	1,07
39,62	38,5	0,966	1,12	2,82%	1,05
49,03	47,8	1,197	1,23	2,52%	1,04
59,04	57,6	1,446	1,44	2,43%	1,04
69,23	67,7	1,699	1,53	2,22%	1,03
79,53	77,8	1,951	1,73	2,18%	1,03

Bibliography

Bishop, T. (2013, 05 21). *Motor Nameplate Letter Code Designations*. (Pumps and Systems) Retrieved 01 03, 2019, from https://www.pumpsandsystems.com/topics/motors/motor-nameplate-letter-code-designations

Economides, M. (n.d.). *Artificial Lift Completion.*

Fiorucci, E., Bucci, G., Ciancetta, F., Gallo, D., Landi, C., & Luiso, M. (2013, 04 13). Variable Speed Drive Characterization: Review of Measurment Techniques and Future Trends. (F. Profumo, Ed.) *Advances in Power Electronics*, 6.

Guo, B., Lyons, W., & Ghalambor, A. (2007). *Petroleum Production Engineering.* Elsevier Science & Technology Books.

Harman, C. (2014, 03 20). *What is a VSD drive*. (VSDs.com) Retrieved 02 17, 2019, from https://www.vfds.com/blog/what-is-a-vf

Hottinger Baldwin Messtechnik GmbH. (2018, January). Mounting Instructions T10F. 14. Darmstadt: Hottinger Baldwin Messtechnik GmbH.

Lake, L., & Clegg, J. (2007). *Petroleum Engineering Handbook - Production Operations Engineering.* Society of Petroleum Engineers.

Lake, L., & Clegg, J. (2007). *Petroleum Engineering Handbook - Production Operations Engineering.* Society of Petroleum Engineers.

Lake, L., & Clegg, J. (2007). *Petroleum Engineering Handbook - Production Operations Engineering.* Society of Petroleum Engineers.

Langbauer, C. (2017). *Artificial Lift Systems Practical - Sucker Rod Pump.* Department of Petroleum and Geothermal Energy Recovery.

LEM HOLDING SA. (2003, Febuary 10). *Current Transducer LT200-S Data sheet.* Retrieved April 14, 2019, from Datasheets: https://www.datasheets.com/datasheet/lt-200-s-sp44-lem-group-15339271

LEM HOLDING SA. (2017, October 17). *LEM Voltage Transducer LV100.* Retrieved April 15, 2019, from LEM: https://www.lem.com/sites/default/files/products_datasheets/lv_100_-_100.pdf

M.A. Reedy, I. E. (2006). Reducing Electric Pumping Consumption in Mature Fields: Case Studies. *SPE Western Regional/AAPG Pacific Section/GSA Cordilleran Section Joint Meeting* (pp. 1-7). Anchorage: SPE.

Siemens. (n.d.). *Effizienzklassen für IEC Netzmotoren*. Retrieved 01 03, 2019, from https://w3.siemens.com/drives/global/de/motor/niederspannungsmotoren/effizienzklassen/seiten/netzmotoren.aspx#Norm_20IEC_20Netzmotoren_20_IEC_2060034_30_1_

Szilas, A. (1985). *Production and Transport of Oil and Gas - Flow Mechanics and Production* (Second completely revised edition ed., Vol. Part A). Elsevier.

Toliyat, A., & Kliman, G. (2004). *Handbook of Electric Motors - Induction Motor Analysis and Design* (Vol. 2nd Edition). Taylor & Francis Group, LLc.

Weiß, H. (2018). *Lecture notes to Measurment and Control.* Leoben: Institute of Electical Engineering.

Acronyms

AI	Analogue Input
CAPEX	Capital expenditure
HP	Horse power
IC	Integrated circuit
IE	International efficiency
NEMA	National Electrical Manufacturers Association
OPEX	Operational expenditure
rpm	Revolutions per minute
SPM	Strokes per minute
VFD	Variable frequency drive
VSD	Variable speed drive

Symbols

A	Amplitude	[-]
c	Mills factor	[-]
$\cos\varphi$	Power factor	[-]
f	Frequency	[Hz]
f_c	Cyclic load factor	[-]
F_{dyn}	Dynamic polished rod load	[N]
$F_{dyn\,max}$	Maximum dynamic polished rod load	[N]
$F_{dyn\,min}$	Minimum dynamic polished rod load	[N]
g	Gravitational accelerations	$[\frac{\mathrm{m}}{\mathrm{s}^2}]$
G_f	Gravitational force of the fluid	[N]
G_g	Gravitational force of the rod string	[N]
h_p	Polished rod length	[m]
I	Current	[A]
I_{avg}	Average current	[A]
I_p	Primary nominal current	[A]
I_{rms}	Root mean square current	[A]
I_s	Secondary nominal current	[A]
j	Imaginary number	[-]
k	Conversion Ration	[-]
K_N	Conversion Ration	[-]
M	Torque	[Nm]
n	Offset	[-]
n	Speed	$[\frac{1}{min}]$
n_s	Synchronous speed	$[\frac{1}{min}]$
η	Efficiency	[-]
η_e	Efficiency of the prime mover	[-]
η_m	Mechanical load factor	[-]
ω	Angular frequency	$[\mathrm{s}^{-1}]$
p	Number of Pole pairs	[-]
P	Power	[kW]

P	Active power	[kW]
P_{cu1}	Power losses from the copper winding	[kW]
P_m	Momentary power	[kW]
P_{fe}	Power losses from the iron core	[kW]
φ	Phase angle	[°]
P_{in}	Power input	[kW]
P_{out}	Power output	[kW]
P_{req}	Required power	[kW]
P_s	Polished rod power	[kW]
Q	Reactive power	[kW]
R	Resistor	[Ω]
R_m	Sensing resistor	[Ω]
R_p	Primary resistor	[Ω]
ρ_f	Density of the fluid	$[\frac{\mathrm{kg}}{\mathrm{m}^3}]$
ρ_s	Density of the sucker rods	$[\frac{\mathrm{kg}}{\mathrm{m}^3}]$
s	Slip	[%]
S	Apparent power	[kW]
t	Time	[s]
U	Voltage	[V]
U_{ref}	Reference voltage	[V]
X	Complex resistance	[Ω]
Y	Admittance	[Ω]
Z	Impedance	[Ω]

List of Figures

List of Graphs

List of Tables